FERMILAB-PUB-03/320-E
October 17, 2003

Results of the Tevatron Higgs Sensitivity Study

CDF and DØ Collaborations

Working Group Members

DØ Group
Levan Babukhadia (Stony Brook)
Wade Fisher (Princeton)
Anna Goussiou (Imperial College)
Boaz Klima(*) (Fermilab) (Chair)
Qizhong Li (Fermilab)
Meenakshi Narain (Boston)
Rich Partridge (Brown)
Flera Rizatdinova (Kansas State)
Chris Tully(*) (Princeton)
Andre S. Turcot (Brookhaven)

CDF Group
John Conway (Rutgers)
Tommaso Dorigo (INFN Padova)
Tom Junk (Illinois)
Martin Hennecke (Karlsruhe)
Joseph Kroll(*) (Pennsylvania) (Co-Chair)
Mario Martinez (Fermilab/Barcelona)
Pete McNamara (Rutgers)
Luca Scodellaro (INFN Padova)
Fumi Ukegawa (Tsukuba)
Brian Winer(*) (Ohio State) (Co-Chair)
Weiming Yao (LBNL)

(*) Contact Persons

In this study, the results from the working group members of each collaboration have been individually reviewed by the corresponding collaborations and approved for public release.

Executive Summary[1]

The Tevatron is currently the only accelerator capable of producing a low mass Higgs boson. Understanding the sensitivity of the Tevatron experiments to either observe or rule out a low mass standard model Higgs boson is important. Several years ago a study based at Fermilab known as the *SUSY-Higgs Working Group* (SHWG) reported on this sensitivity. Now that the CDF and DØ collaborations have collected Run IIA data samples that exceed the Run I samples, a reevaluation of the Higgs sensitivity can be carried out using the experience of the Run IIA data and the detailed detector simulations. In early 2003, the Office of Science of the Department of Energy requested that the Tevatron experiments carry out such a reevaluation. The CDF and DØ collaborations agreed to form working groups for this study. In order to produce the result in a timely manner, the two working groups divided the effort. The DØ working group focused on the $\nu\bar{\nu}b\bar{b}$ final state, primarily produced via $p\bar{p} \rightarrow ZH \rightarrow \nu\nu b\bar{b}$, while the CDF working group focused on the $\ell\bar{\nu}b\bar{b}$ final state, primarily produced via $p\bar{p} \rightarrow WH \rightarrow \ell\nu b\bar{b}$. These studies assumed the Run IIB detector upgrades, including the silicon vertex detectors, which were under construction at that time. While this manuscript was in progress, the Fermilab Director canceled the upgrades of the silicon vertex detectors. This decision impacts the results of this study primarily through the capabilities of the experiments to tag bottom quarks from the decay of the Higgs boson. The b-quark tagging using the current silicon detectors will likely degrade due to radiation damage when the integrated luminosity exceeds $\sim 4\,\mathrm{fb}^{-1}$. We are in the process of determining the sensitivity using the current silicon detectors for the duration of Run II.

The Higgs boson can be produced via several mechanisms at the Tevatron (Figure 2). The process with the largest cross section is $gg \rightarrow H$. However, in the low mass region ($100 < m_H < 140\,\mathrm{GeV}/c^2$), where the Higgs decays primarily to a $b\bar{b}$ pair (Figure 3), this channel is overwhelmed with background from generic QCD processes. The more promising modes at the Tevatron are the production of the Higgs boson in association with either a W or Z boson. The decays $W \rightarrow \ell\nu$ and $Z \rightarrow \nu\nu$, $\ell^+\ell^-$ provide an important signature for improving the signal-to-background. In addition, tagging the two b-quark jets by the presence of displaced vertices gives a second important handle. Despite these two unique features, substantial backgrounds still exist. The primary sources of background are $t\bar{t}$, $W/Zb\bar{b}$, WZ, ZZ, single top quark production and, in the case of the $\nu\bar{\nu}b\bar{b}$ channel, background from QCD processes. In most of these backgrounds *real* leptons from W/Z decays and *real* pairs of b quarks are present in the final state. Therefore, we must rely on the detailed event characteristics in order to improve the signal-to-background. In this regard we start with basic event selection and then turn to more advanced techniques such as neural networks to provide our final event sample. The final step in the analysis is to examine the invariant mass spectrum of the two identified b-quark jets. In one important difference relative to the SHWG report, we do not simply count events in a mass window around the theoretical Higgs boson mass. Instead we fit the $m_{b\bar{b}}$ distribution to a combination of signal and background. Studies have shown that this gives us an increase in sensitivity of about 20%, meaning we can make the same statistical statement with 20% less integrated luminosity.

The $\ell\bar{\nu}b\bar{b}$ analysis has a basic event selection that follows the expected event topology. First, we select events that are consistent with the decay of a W boson to a charged lepton

[1]Figure and table numbers refer to the main document.

(e, μ, single prong τ) and missing energy caused by the neutrino. Second, since the Higgs boson is expected to decay primarily to a pair of b quarks, we require the presence of jets. We search these jets for evidence of the production of the relatively long-lived hadrons containing b quarks by looking for indications of secondary vertices or for tracks that do not extrapolate back to the primary $p\bar{p}$ interaction point. The lepton and b tagging is extrapolated through the largest fiducial range we think is achievable. For $m_H = 115\,\mathrm{GeV}/c^2$, the overall acceptance is 6.6%, yielding 2.9 events/fb^{-1} when folding in the production cross section and branching ratio of the Higgs boson decay. The rates of backgrounds are considerably higher. The two largest backgrounds, $Wb\bar{b}$ and $t\bar{t}$, give 108 and 47 events/fb^{-1}, respectively. There are 34 events from the other background sources. These event rates are for the full $m_{b\bar{b}}$ spectrum. If we restrict ourselves to a mass window around m_H, we find 2.5 signal events and 30 background events (Table 3). As a final step, a neural network study is performed to further reject background events. Efficiencies for the backgrounds and signal to satisfy a neural network selection criteria were determined using the DØ analysis infrastructure (Table 20). The neural network was most effective at rejecting $t\bar{t}$ events and reduced the total background from 30 to 17 events, while leaving the signal at 2.4 events.

The $\nu\bar{\nu}b\bar{b}$ analysis has a basic selection that begins with identifying events with a large amount of transverse missing energy caused by the two neutrinos. Several quality criteria are imposed to reduce background in which the missing energy is caused by detector effects. In addition, events that have a final state object that is consistent with a high p_T lepton are rejected. As in the $\ell\bar{\nu}b\bar{b}$ channel, the Higgs boson is expected to manifest itself as two b-quark jets. Therefore, the events are required to have two high transverse energy jets that are consistent with coming from b quarks. In the case of the $\nu\bar{\nu}b\bar{b}$ analysis, the neural network approach was an integral part of the analysis. It provides important rejection against events containing top quarks. For $m_H = 115\,\mathrm{GeV}/c^2$, the overall acceptance is 16%, yielding a signal of 4.3 events/fb^{-1}. Part of this signal is due to WH production, which has a higher cross section than ZH. If the lepton from the W decay is lost, WH production has the topology of the $\nu\bar{\nu}b\bar{b}$ final state (Tables 7–9). The largest backgrounds, QCD, $W/Zb\bar{b}$ and ZZ, give 61, 22, and 11.5 events/fb^{-1}, respectively. The QCD background is the hardest background to estimate. The determination of this background benefitted significantly from having Run IIA data. There are 19.5 events from the other background sources. Once again these rates are for the full $m_{b\bar{b}}$ spectrum. If we restrict ourselves to a mass window around m_H, such a window would yield 3.8 signal events and 19.6 background events (Table 20).

As previously mentioned one important difference between this study and the SHWG study was the use of the full $m_{b\bar{b}}$ mass spectrum (Figures 21–22). The $m_{b\bar{b}}$ distribution is fit to a combination of signal and background. The fit is used to either observe an excess of events in the signal region or a lack of signal at some confidence level. We evaluate our sensitivity to the Higgs boson using two different approaches. The first is a Bayesian approach similar to that used in the SHWG report. The second is a method developed at LEP, called the CL$_s$ method. Both methods give comparable results. In order to quantify our sensitivity to observing or ruling out the Higgs boson, we establish "luminosity thresholds." These thresholds are defined by running many pseudoexperiments based on the $m_{b\bar{b}}$ distributions and the predicted event yields. These pseudoexperiments include Poisson fluctuations in both the signal and the backgrounds. For a given amount of integrated luminosity, we can determine the fraction of pseudoexperiments that satisfy some statistical statement, such as

exclusion at the 95% confidence level (CL) or observation of a three standard deviation (3σ) excess or a five standard deviation (5σ) excess. We perform this evaluation over a wide range of possible integrated luminosities and select our threshold as the luminosity where 50% of the pseudoexperiments satisfy the condition. These thresholds depend on the Higgs boson mass (Table 21). There is a wide range of possible outcomes as illustrated in Figures 19 and 20.

Figure 24 summarizes the luminosity thresholds as a function of m_H for the 95% CL exclusion, 3σ excess, and 5σ excess. The curves from this study represent the expected statistical power of the data only; no systematic effects have been included. The figure also shows the results from the SHWG report. Fits to the electroweak data indicate the existence of a light mass Higgs boson, possibly just above the lower mass limit established by LEP. If the mass of the Higgs boson is very close to $115\,\mathrm{GeV}/c^2$, the Tevatron experiments should be able to observe a 3σ excess with about $\sim 3\,\mathrm{fb}^{-1}$. It would take about $8\,\mathrm{fb}^{-1}$ for a 5σ excess. Similarly, with $\sim 4\,\mathrm{fb}^{-1}$ the Tevatron experiments should be able to exclude the Higgs boson up to about $m_H = 130\,\mathrm{GeV}/c^2$, if it is not present. We have not included the impact of systematic uncertainties in this study. Including the effects of systematics will push the luminosity thresholds higher. We have reviewed the major sources of systematic errors, and we discuss how we might be able to evaluate them in the future (Section 8). Some of these uncertainties have been quantified. Specifically, we have studied the impact of uncertainties on the event normalization (Table 22). For example, a 10% uncertainty on the signal and background rates leads to a 5%, 15%, and 20% rise in the luminosity thresholds for 95% CL exclusion, 3σ, and 5σ excess at a Higgs mass of $m_H = 120\,\mathrm{GeV}/c^2$.

The results of this study show a reduction in the amount of integrated luminosity required to search for the Higgs boson at the Tevatron collider relative to the previous SUSY-Higgs Working Group Study. A number of important improvements were possible using the data collected so far in Run IIA and from the full detector simulations, which include the effects of the high luminosity environment. First, all the event selection efficiencies were tied to the Run IIA detector simulations and the data itself. Second, additional analysis of the dijet mass resolution seems to indicate that a mass resolution of 10% may be achievable (Section 5). In addition, the QCD background estimate for the $\nu\bar{\nu}b\bar{b}$ channel was substantially improved by using the Run II data. Finally, the use of neural networks reduces the background, especially $t\bar{t}$, while maintaining a large portion of the signal. Controlling the systematic errors, especially $m_{b\bar{b}}$ shape uncertainties, will be important. We have presented a discussion of these systematics and how they may be studied. Further developments on the Higgs search are certain to occur in both experiments.

1 Introduction

The Standard Model of fundamental interactions has had at its origins a mechanism for generating mass in elementary particles[1]. Direct and indirect searches conducted over the last 30 years provide compelling evidence for a low mass Higgs boson. The search for this particle and any other manifestation of new physics at the electroweak scale is the principal driving force behind the experimental high energy physics program. The possibility of contributing to this physics at the Tevatron collider warrants careful review.

In 1998 physicists from the CDF and DØ collaborations and the Fermilab Theoretical Physics Department organized a workshop to study the potential for discovering the Higgs boson in Run II of the Fermilab Tevatron. The results of this workshop are documented in a paper entitled *Report of the Higgs Working Group of the Tevatron Run 2 SUSY-Higgs Workshop* [2]. Their findings are summarized in Figure 1.

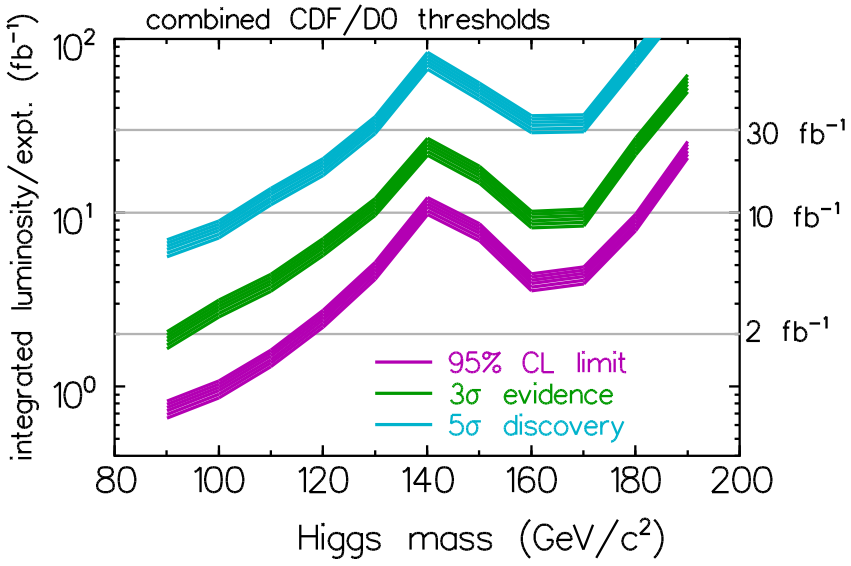

Figure 1: This figure summarizes the findings of the SUSY-Higgs Working Group study. The vertical axis is the required integrated luminosity *per experiment* for three different levels of Higgs search sensitivity, 95% CL exclusion, 3σ evidence and 5σ discovery.

Several event topologies were examined for sensitivity to a standard model Higgs boson signal. The most promising modes were associated production of a Higgs boson and an intermediate vector boson: (1) $p\bar{p} \to WH$, followed by $W \to \ell\nu$, where $\ell = e$ or μ and $H \to b\bar{b}$, and (2) $p\bar{p} \to ZH$, with $Z \to \nu\bar{\nu}$, and $H \to b\bar{b}$. The studies were based on a parameterized simulation known as the "SHW simulation," which was used to estimate the response of a generic Tevatron detector. Comparisons of the SHW simulation and Run I data were used to validate this approach, and efficiencies measured in data, such as the efficiency for tagging b-flavored jets based on the presence of a displaced secondary vertex, were used to make the estimates of signal acceptance and background rates as realistic as possible.

It is now four years after the completion of the SUSY-Higgs Working Group (SHWG) study. Run II of the Fermilab Tevatron is under way, and both experiments have accumulated

enough data to allow a better evaluation of our potential sensitivity to the Higgs boson. Hit-level GEANT-based simulations of the CDF and DØ Run II detectors are available. They have been compared with current data, resulting in more reliable estimates of the signal efficiency and the background contamination. Full simulations of b tagging in the extended Run IIB detectors and projected luminosities are also available and have been tied to Run II data. Trigger rates have been measured in the data and can be extrapolated more reliably to higher luminosities. The running conditions of the Tevatron have also evolved. The plan to upgrade the Tevatron to run with a crossing time of 132 ns has been abandoned. Staying with a crossing time of 396 ns means that the rate of multiple interactions will be higher and the effect of high event occupancies may be more relevant than anticipated in the SHWG study.

In order to make an improved estimate of the Higgs boson discovery potential of the Tevatron program, the CDF and DØ collaborations agreed to conduct a new study together. To carry out the initial reevaluation in an expedient manner, the collaborations decided to divide the work. Each collaboration focused on one of the two most promising channels: CDF examined $p\bar{p} \to WH$, with $W \to \ell\nu$ and $H \to b\bar{b}$, while DØ investigated $p\bar{p} \to ZH$, with $Z \to \nu\bar{\nu}$ and $H \to b\bar{b}$. Each collaboration established a task force to perform these studies. Two advanced methods of analysis and reconstruction are applied in this study. The first is the study of the dijet mass resolution. The second is the use of neural network techniques for event selection. For both the $\ell\bar{\nu}b\bar{b}$ and $\nu\bar{\nu}b\bar{b}$ analyses, the b-tagging efficiency from the silicon vertex detectors is the most important factor in setting the overall rate of detecting Higgs bosons for a given luminosity. The Run IIB b-tagging efficiencies and geometries are applied in this study. We assumed instantaneous luminosities as high as $\mathcal{L} = 4 \times 10^{32}\,\mathrm{cm}^{-2} \cdot \mathrm{s}^{-1}$.

The cross section for standard model Higgs boson production in $p\bar{p}$ collisions at $\sqrt{s} = 1.96\,\mathrm{TeV}$ is shown in Figure 2; the branching fractions are shown in Figure 3. We use the production cross section and branching fractions from these calculations in our determination of our sensitivity to the Higgs boson.

We begin the document by reviewing the CDF $\ell\bar{\nu}b\bar{b}$ analysis in Section 2 and the DØ $\nu\bar{\nu}b\bar{b}$ analysis in Section 3. In Section 4 we discuss a cross check of the $\ell\bar{\nu}b\bar{b}$ analysis using the DØ detector simulation and analysis tools, and we quantify the sensitivity improvement to the $\ell\bar{\nu}b\bar{b}$ analysis from using a neural network. Section 5 reviews the current understanding of the dijet mass resolution, a key component of both analyses. The statistical sensitivity of the Tevatron Higgs boson search is presented in Sections 6 and 7. A discussion of the possible systematic errors of the study appears in Section 8. Section 9 contains conclusions and a summary.

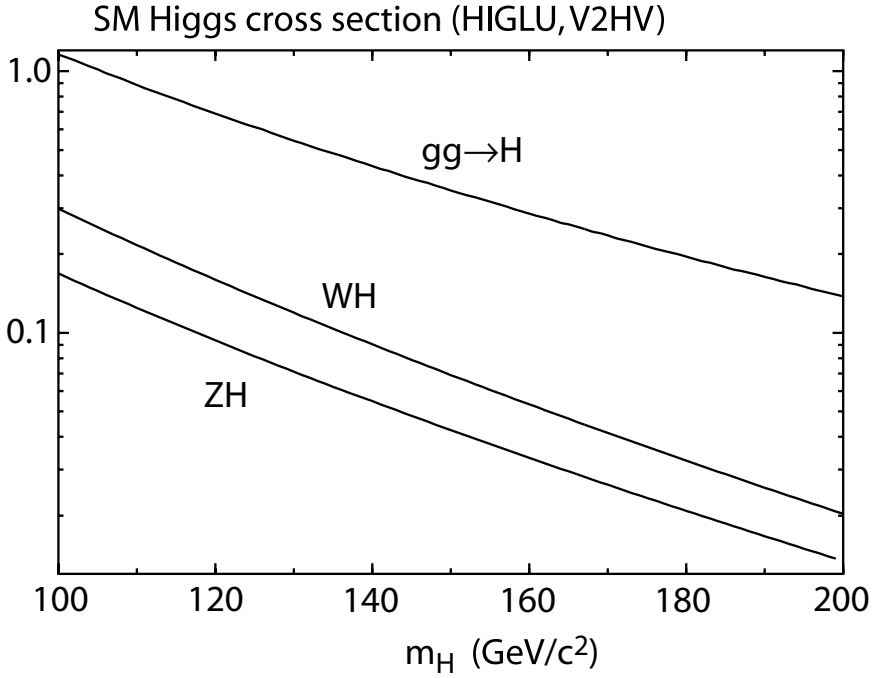

Figure 2: The production cross section in picobarns for the standard model Higgs boson in $p\bar{p}$ collisions at $\sqrt{s} = 1.96\,\mathrm{TeV}$. These cross sections are based on a calculation by T. Han and S. Willenbrock[3].

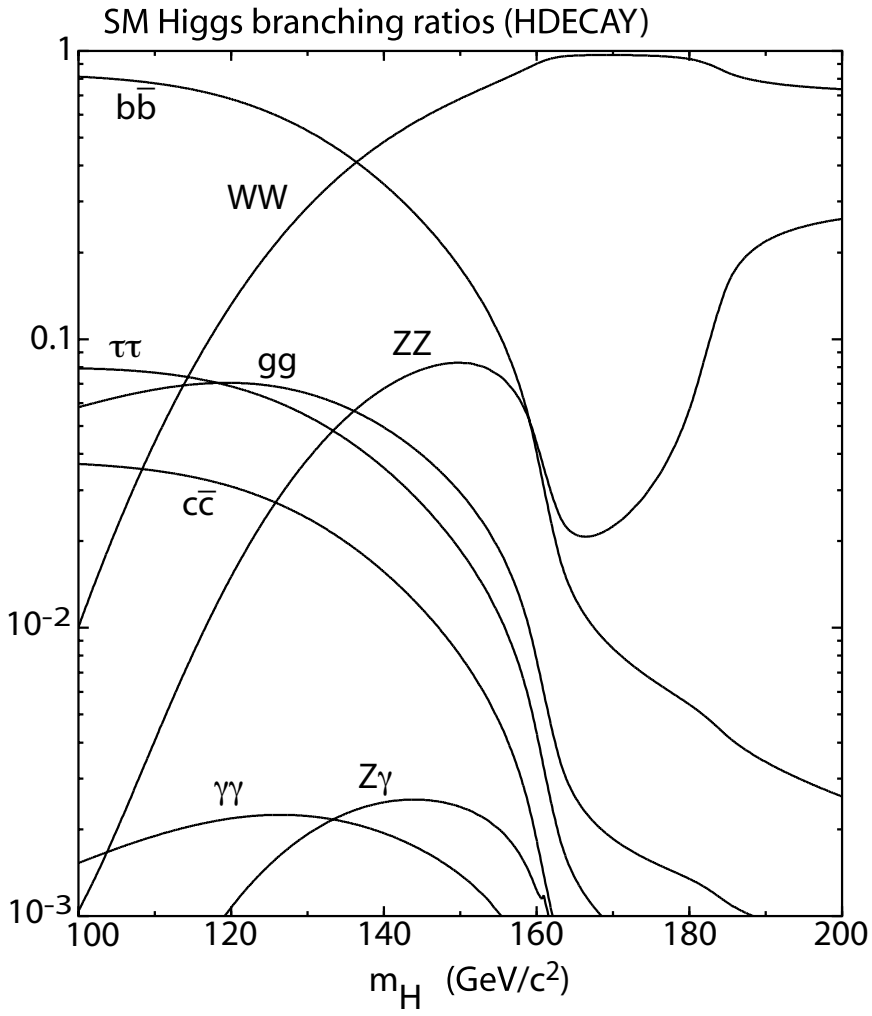

Figure 3: The branching fractions of the standard model Higgs boson. These branching fractions are calculated using the computer program `HDECAY`[4].

2 $\ell\bar{\nu}b\bar{b}$ Analysis

We will begin by discussing the search for the process $p\bar{p} \to WH$, with $W \to \ell\nu$, and $H \to b\bar{b}$, where ℓ means e, μ, or τ. To select this process, we require an isolated electron, an isolated muon, or an isolated track with high transverse momentum (p_T) and a large momentum imbalance or missing energy $\not\!\!E_{\rm T}$, which are produced by the decay of the W. To select signal events, we require the presence of two or three jets. Two of these jets are required to be consistent with having been produced by the relatively long-lived b quark (b tagged). Heavy quark decay is identified by requiring either that the jet contain a displaced secondary vertex or tracks that are not consistent with originating from the primary $p\bar{p}$ interaction.

Our study considers Higgs boson masses in the range $110 < m_H < 140\,\mathrm{GeV}/c^2$. The product of the production cross section of WH multiplied by the branching fractions of $W \to \ell\nu$ (0.33) and $H \to b\bar{b}$ ranges from 54 fb for $m_H = 110\,\mathrm{GeV}/c^2$ to 10 fb for $m_H = 140\,\mathrm{GeV}/c^2$.

The dominant backgrounds to associated Higgs boson production and decay are due to physics processes that produce the same signature, not instrumental backgrounds. These processes include

- $\boldsymbol{W}$ **+ jets**: $p\bar{p} \to W + g, g \to b\bar{b}, c\bar{c}$, with a production cross section of $\sigma \sim 10$'s of pb;
- $\mathbf{t\bar{t}}$: $p\bar{p} \to t\bar{t} \to W^+bW^-\bar{b}$, with a production cross section of $\sigma \sim 7$ pb;
- **Single top**: $p\bar{p} \to t\bar{b} \to W^+b\bar{b}$, with a production cross section of $\sigma \sim 3$ pb; and
- **WZ**: $p\bar{p} \to WZ \to \ell\nu b\bar{b}$, with a production cross section of $\sigma \sim 3$ pb.

These backgrounds produce the same signature: $Wb\bar{b}$, and if the selection is based on the finding a W and two b quarks, then these backgrounds are irreducible. Improving the efficiency of the trigger, W identification or b identification affects the signal and background processes almost equally and only helps improve the signal significance by increasing $S/\sqrt{B}$. Since the cross sections for these irreducible backgrounds are so much larger, it is necessary to enhance the signal either using kinematic criteria (possibly utilizing neural network techniques) or by reconstructing the Higgs boson directly by examining the invariant mass distribution of the two b-tagged jets, $m_{b\bar{b}}$. The resolution of $m_{b\bar{b}}$ is the crucial experimental parameter in this search.

2.1 Basic Event Selection

Our selection is similar to that of the SHWG. In the baseline event selection presented in this section, no additional optimization of the selection criteria has been attempted. In Section 4 we investigate the added sensitivity obtained by using a neural network after the baseline selection. The added background rejection from the neural network is included in the final sensitivity. We began with the CDF Run IIA lepton selection (February 2003) and displaced vertex b-tagging algorithm as our baseline selection and then consider potential improvements and extensions of these established algorithms. For the leptons, our baseline uses central electrons ($|\eta| < 1.1$) and central muons ($|\eta| < 1.1$). We used Monte Carlo simulations to explore the impact of expanding our lepton coverage to the endcap calorimeter ($1 < |\eta| < 2$)

and the intermediate muon detector ($1.1 < |\eta| < 1.5$). The basic event selection criteria prior to b tagging are as follows:

- One lepton with $p_T > 20\,\mathrm{GeV}/c$
  - where lepton means electron, muon, or isolated track;
  - standard selection criteria are applied to the leptons;
  - any event with two or more leptons is vetoed.
- $\not\!\!E_{\mathrm{T}} > 20\,\mathrm{GeV}$ (uncorrected)
  - when the lepton is an isolated track, the $\not\!\!E_{\mathrm{T}}$ requirement is increased to $\not\!\!E_{\mathrm{T}} > 35\,\mathrm{GeV}$.
- Remove $Z \to \ell^+\ell^-, \ell = e, \mu$
  - includes $76 < m_{\ell\ell} < 106\,\mathrm{GeV}/c^2$.
- A tight jet satisfies $E_T > 10$ GeV, $|\eta| < 2.0$ (uncorrected, cone= 0.4).
- A loose jet satisfies $E_T > 10$ GeV, $|\eta| < 2.4$ (uncorrected, cone= 0.4).
- The jet requirements are 2 or 3 tight jets.
- The event must satisfy the following additional kinematic requirements:
  - one tight jet must have $E_T > 25\,\mathrm{GeV}$;
  - no third jet with $E_T > 20\,\mathrm{GeV}$ is allowed;
  - no second isolated track with $p_T > 10\,\mathrm{GeV}/c$ is allowed.

The last additional kinematic selection requirements serve to reduce the $Wq\bar{q}$ (25 GeV requirement), $t\bar{t}$ (no hard third jet), and Z decays (no second isolated track).

To study the signal acceptance for these selection criteria, we produced Monte Carlo samples of $p\bar{p} \to WH$ using the `ALPGEN` event generator followed by `GEANT` simulation of the Run IIA detector and production. All decays of the Higgs boson and W boson are allowed. The results of applying the above basic selection to the Higgs boson Monte Carlo samples are shown in the top portion of Table 1. In this table, only events with $W \to \ell\nu$, $\ell = e, \mu, \tau$, and $H \to b\bar{b}$ are considered. All extensions to the primary lepton coverage are included in this acceptance. The WH production cross sections and $H \to b\bar{b}$ branching fractions are taken from the references given in Section 1.

We use `ALPGEN`, `HERWIG`, and `PYTHIA` Monte Carlo samples to evaluate the backgrounds. The selection criteria acceptance for the backgrounds is shown in the top portion of Table 2. The expected background rates from $W+$ jets production is normalized directly from the data [5]. The Monte Carlo is used to establish (*i*) the fraction of observed events that are $Wb\bar{b}$, $Wc\bar{c}$, and (*ii*) the b-tagging efficiency of these events.

Higgs Mass (GeV/c^2)	110	115	120	130	140
Cross Section (pb)	0.216	0.186	0.160	0.119	0.0902
BR ($WH \to \ell\nu b\bar{b}$)	0.770×0.33	0.732×0.33	0.679×0.33	0.527×0.33	0.344×0.33
1 e, μ, or isol. trk	42	42	42	42	43
$\not\!\!E_{\rm T} > 20\,{\rm GeV}$	89	89	89	89	89
Pass Z Veto	99	99	99	99	99
Jet Selection	77	78	80	80	80
Kinematic Selection	84	84	84	84	82
≥ 1 b-tagged jet	66	66	67	68	69
2 b-tagged jets	28	28	29	30	31
Acceptance	6.7	6.6	7.1	7.4	7.7
Trigger Efficiency	95	95	95	95	95
Events in 1 fb^{-1}	3.51	2.86	2.44	1.47	0.76

Table 1: The acceptance (%) and yield per fb^{-1} for WH events as a function of Higgs boson mass. The event yield is after all extensions to primary lepton identification and b tagging. The two b-tagging efficiencies are each relative to events satisfying all other selection criteria and, therefore, should not be multiplied. The branching ratio (BR) is the product of BR($H \to b\bar{b}$) multiplied by BR($W \to \ell\bar{\nu}$).

2.2 b Tagging

We require that two jets have evidence of B hadron decay in order to reduce the backgrounds and to remove combinatorical ambiguity when reconstructing the invariant mass of the Higgs boson candidates. Since the dominant physics backgrounds contain a $b\bar{b}$ pair, there is great potential to increase $S/\sqrt{B}$ by requiring only one b tag. This extension has not been considered in this analysis. We have, however, allowed the second b tag to satisfy less restrictive selection criteria (loose) than the first tag, thereby enhancing $S/\sqrt{B}$ as much as possible.

We used two b-tagging algorithms:

1. **Tight:** this is a displaced vertex tag with an event-by-event primary vertex reconstruction. All channels in the silicon detector simulation were live and the silicon was perfectly aligned.

2. **Loose:** this algorithm determines the combined probability that the tracks within a jet are consistent with the primary vertex. A loose tag required this probability to be less than 5%.

The single tag efficiency reported in Table 1 and Table 2 is the efficiency for finding one or more tight tags. In the SHWG study, this efficiency was increased by 10% to account for additional b tags based on leptons from semileptonic B hadron decay. These soft lepton tags have not been included in this analysis because they add additional background that we have not evaluated.

For this study, we required one tight b tag and a second b tag that is tight or loose. The efficiency of the tight b tag, loose b tag, and their combination as a function of jet transverse

Background Source	$Wb\bar{b}$	W$c\bar{c}$	$W+$ light q	$t\bar{t}$	$t(W^*)$	$t(Wg)$	WZ
Cross Section (pb)	na	na	na	7.0	0.80	2.24	3.2
Branching Ratio	na	na	na	56	33	33	33
1 e, μ or Isol Trk	na	na	na	32	38	40	39
$\not\!\!E_{\rm T} > 20\,{\rm GeV}$	na	na	na	90	89	89	89
Pass Z Veto	na	na	na	95	99	99	91
Jet Selection	na	na	na	42	74	63	53
Kinematic Selection	na	na	na	46	83	83	79
≥ 1 b-tagged jet	56	11	0.8	62	67	46	16
2 b-tagged jets	21	7	0.3	24	31	4.1	4
Acceptance	na	na	na	1.26	6.3	0.74	0.58
Trigger Efficiency	na	na	na	95	95	95	95
Events in 1 fb^{-1}	108	3.5	3.8	46.7	15.9	5.24	5.90

Table 2: The acceptance (%) and yield for background processes in the WH channel. The event rates are without any mass window and include all extensions to primary lepton identification and b tagging. The $Wb\bar{b}$, $Wc\bar{c}$, and $W+$ light q are normalized to the rate of $W+$ jet events observed in the data. The Monte Carlo is used to determine the fraction of heavy flavor jets (*e.g.*, the fraction of $Wb\bar{b}$ relative to $W+$ jets) and the tagging efficiency for these events. Therefore, the individual efficiencies are not given. The two b-tagging efficiencies are each relative to events satisfying all other selection criteria and therefore should not be multiplied. The branching ratio is BR($W \to \ell\bar{\nu}$) and includes combinatorical factors.

energy are shown in Figure 4. The efficiency was measured in the central ($|\eta| < 1.0$) portion of the CDF detector. We describe the b-tagging efficiency as a function of jet E_T, $\epsilon(E_T)$, using a hyperbolic tangent:

$$\epsilon(E_T) = A \tanh\left[\frac{E_T + B}{C}\right],$$

with $A = 0.707$, $B = 0.729\,{\rm GeV}$, and $C = 23.2\,{\rm GeV}$ for the OR of tight and loose b tags.

Currently, the efficiency of these algorithms falls off with increasing $|\eta|$. The solid lines in Figure 5 shows this dependence. However, we assume with the development of forward stand-alone silicon tracking, we will be able to extend these algorithms to larger $|\eta|$. To evaluate this extension in η, we examine the η distribution of b tags in four bins of jet E_T: $10 < E_T < 20\,{\rm GeV}$, $20 < E_T < 30\,{\rm GeV}$, $30 < E_T < 40\,{\rm GeV}$, $40 < E_T\,{\rm GeV}$, using the WH Monte Carlo samples at $m_H = 115\,{\rm GeV}/c^2$. We take the η dependence shown for the current algorithms and "stretch" the dependence to larger η. The dependence is shown by the dashed lines in Figure 5. Since the $|\eta|$ distribution for b quarks is strongly peaked toward low $|\eta|$, our total tagging efficiency is not strongly dependent on the decrease of efficiency with $|\eta|$.

The efficiencies for signal and background to satisfy a single and a double b tag are listed in Table 1 and Table 2. The numbers in the rows labeled "≥ 1 b-tagged jet" correspond to the efficiency for finding at least one tight tag. The numbers in the rows labeled "2 b-tagged jets" correspond to the efficiency for finding one tight tag and a second tag that may be

	No Mass Window	Mass Window
WH ($m_H = 115$ GeV/c^2)	2.86	2.50
$Wb\bar{b}$	108.	13.8
$Wc\bar{c}$	3.5	0.44
Wqq	3.8	0.49
$t\bar{t}$	46.7	10.0
$t(W^*)$	15.9	3.5
$t(Wg)$	5.40	1.1
WZ	5.90	1.0
Total Bkg	189.	30.3
$S/\sqrt{B}(@m_H = 115)$	0.21	0.45
S/B ($@m_H = 115$)	0.015	0.082

Table 3: Summary of the event yields for signal and background. The first column shows the events per fb^{-1} without an $m_{b\bar{b}}$ window. The second column show the event count inside a mass window defined by $100 < m_{b\bar{b}} < 136\,\mathrm{GeV}/c^2$.

either a tight or loose tag; *n.b.*, both of these efficiencies are relative to the sample after all selection criteria and prior to any b tagging. The single and double b-tagging efficiencies should not be multiplied. The fake rate for false tags of light quarks and gluons is taken as $\sim$0.5% for tight tags and $\sim$2.5% for loose tags.

2.3 Summary of Yields: Signal and Background

The summary of the expected numbers of events per fb^{-1} for the signal process at five different values of m_H and for the dominant background processes are shown in the bottom portions of Table 1 and Table 2. These yields include all the extensions beyond the current Run IIA analyses. These extensions are summarized as follows:

- we extend the primary lepton coverage into the endplug calorimeters and the intermediate muon detectors. This extension impacts each of the processes slightly differently; the typical increase in lepton acceptance is 30% relative to the current acceptance for Run II central leptons.
- We allow the primary lepton to be an isolated high p_T track. This provides an approximate 40% increase relative to central leptons.
- We extend the b tagging to higher η, which increases the double b-tagging efficiency by about 50% (relative) for the signal and the two largest backgrounds ($Wb\bar{b}$, $t\bar{t}$).

Development of these extensions is in progress, and they should become part of the standard Run II analyses in the future.

The yield numbers in Table 1 and Table 2 are without any mass window around the reconstructed Higgs boson. The SUSY-Higgs Working Group used a mass window to perform

a counting experiment. Table 3 shows the total event yields compared to the event yields in a mass window around $m_H = 115\,\mathrm{GeV}/c^2$. The mass window is $100 < m_{b\bar{b}} < 136\,\mathrm{GeV}/c^2$, which encloses approximately 90% of the signal.

The baseline selection described above does not include any advanced analysis techniques such as neural networks. Such techniques have been shown to reduce the backgrounds while maintaining a large amount of signal. A neural network was used in a Run I CDF Higgs boson search; the limits obtained using the neural network were found to be equivalent to the expected limits that would be achieved if the data sample was increased by a factor of 1.6 and the neural network was not employed. The $\nu\bar{\nu}b\bar{b}$ analysis presented in Section 3 uses a neural network to improve the sensitivity in that channel. Section 4 gives the results of applying the same neural network with almost identical variables to the $\ell\bar{\nu}b\bar{b}$ channel, and confirms the integrated luminosity scaling factor of 1.6 found in the CDF Run I analysis. This factor along with the efficiencies found in this section will be used when evaluating the total sensitivity in Section 6.

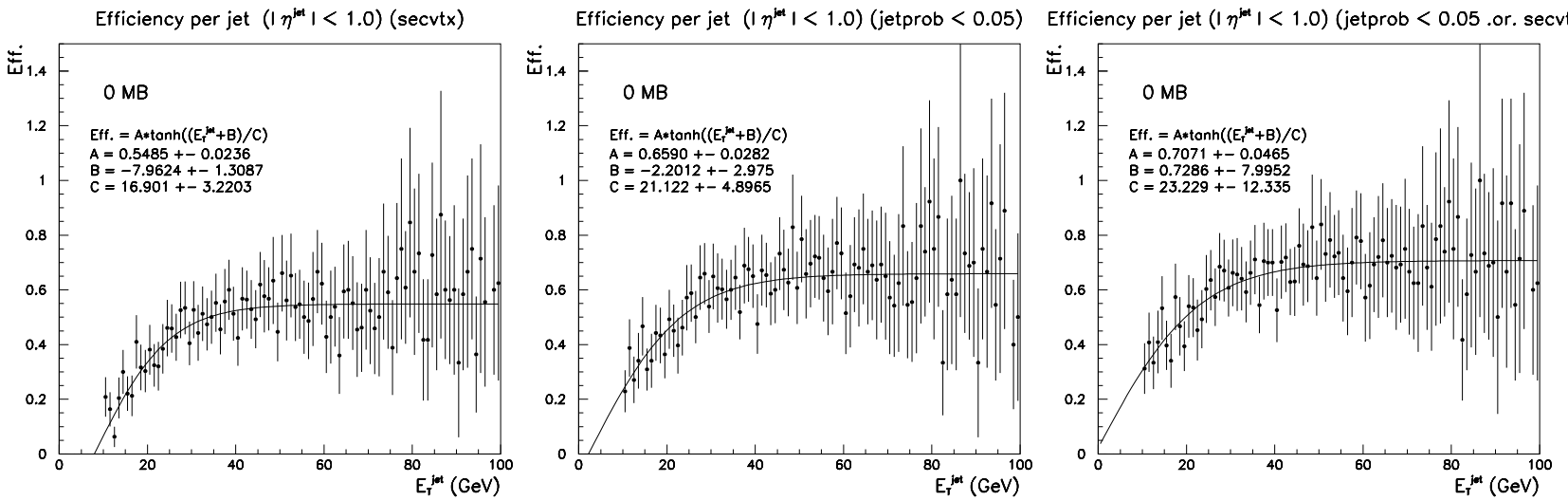

Figure 4: The b-tagging efficiency as a function of b jet E_T for the tight b-tagging criteria (left), the loose b-tagging criteria (center), and their combination (logical `.OR.`, right).

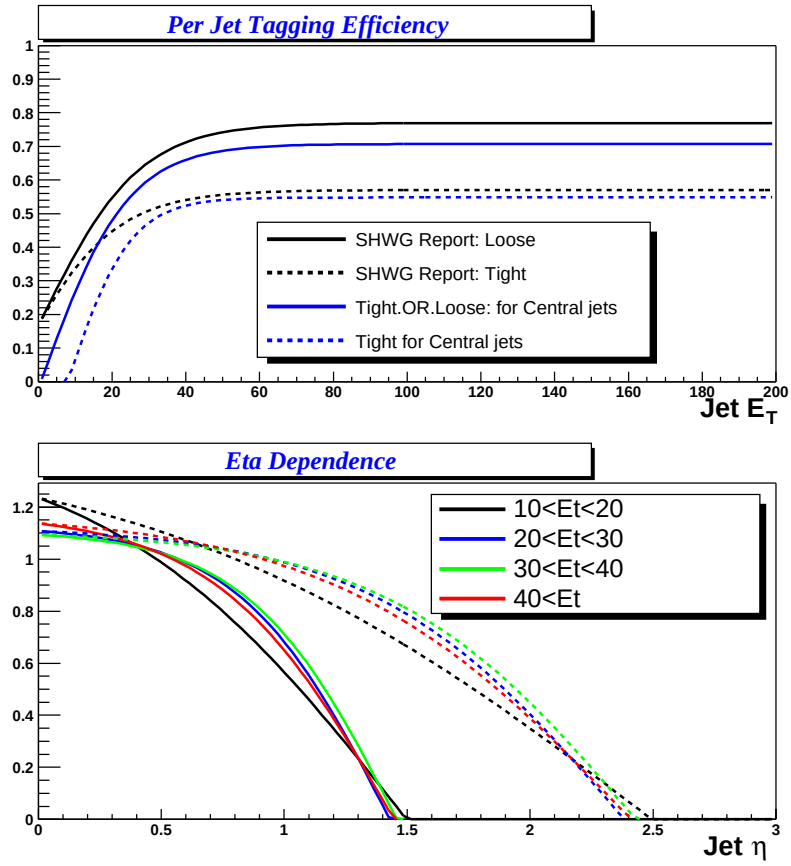

Figure 5: The b-tagging efficiency as a function of b jet transverse energy E_T and as a function of η. In the lower plot, the solid lines represent fits to the Run IIA $|\eta|$ dependence. The dashed lines represent the extension to larger $|\eta|$. The SHWG assumed the η dependence was flat out to 2.0.

3 $\nu\bar{\nu}b\bar{b}$ Analysis

The $\nu\bar{\nu}b\bar{b}$ analysis channel searches for the presence of large missing transverse energy and two identified b-quark jets. This channel selects events from the process $p\bar{p} \rightarrow ZH$, with $Z \rightarrow \nu\bar{\nu}$, and $H \rightarrow b\bar{b}$. There is also a substantial efficiency for selecting events from the process $p\bar{p} \rightarrow WH$, with $W \rightarrow \ell\nu$ and $H \rightarrow b\bar{b}$, where the lepton is not identified in the event.

3.1 Signal and Background Topologies

The $ZH \rightarrow \nu\nu b\bar{b}$ decay topology consists of a purely hadronic signature. A search for this process begins with requiring two or more high-p_T calorimeter jets and a transverse momentum imbalance consistent with a boosted Z boson decaying to neutrinos. The presence of any leptons well separated from the jets is inconsistent with this topology and events containing isolated leptons are vetoed. Furthermore, two of the jets must have properties compatible with containing a b quark (*i.e.*, b-tagged). Tagging of b-quark jets is performed by requiring the jet to contain tracks inconsistent with originating from the primary $p\bar{p}$ vertex.

Any process that produces a dijet plus missing transverse energy ($\not\!\!E_{\rm T}$) signature is a possible background to a $ZH \rightarrow \nu\nu b\bar{b}$ search. This includes events in which a high-energy lepton is misidentified or undetected, resulting in a large $\not\!\!E_T$. However, of the many background processes which can mimic the signal topology, only the following are significant:

- QCD heavy flavor production
- $t\bar{t} \rightarrow W^+ bW^-\bar{b}$
- W/Z + jets
- $WZ \rightarrow \ell\nu b\bar{b}$
- $ZZ \rightarrow \ell\ell b\bar{b}, \nu\bar{\nu}b\bar{b}$
- Single top production

The most significant distinguishing feature of these background events is the reconstructed $b\bar{b}$ mass, $m_{b\bar{b}}$. The distribution of $m_{b\bar{b}}$ for signal events is expected to peak near the Higgs boson mass. However, QCD production of $b\bar{b}$ pairs produces a distribution of $m_{b\bar{b}}$ peaked at low mass and falling at higher masses. The WZ/ZZ backgrounds produce a peak in $m_{b\bar{b}}$ near the Z mass, and the events containing top quarks produce a distribution of $m_{b\bar{b}}$ that rises from low mass and falls off slowly at high mass. A discussion of the dijet mass resolution can be found in Section 5.

3.2 Trigger

The original Run II Higgs/SUSY study did not consider triggering efficiencies. It was implicitly assumed that events passing the offline selection would be triggered on with 100% efficiency. The validity of this assumption has been examined in a study of the Level 1

and Level 2 trigger [6]. This new study utilizes Run IIA data to estimate the trigger rates and Monte Carlo to simulate the signal efficiency. The Level 2 Silicon Track Trigger (STT) performance is a parameterization based on fully simulated events [7].

The triggering strategy relies on an inclusive approach at Level 1 where all associated production channels are triggered on using a single calorimeter trigger. The Level 2 trigger scheme combines global event properties with evidence of b-jet production. The combined Level 1/Level 2 trigger efficiencies are summarized in Table 4. The efficiencies do not include the effect of purely leptonic triggers.

L1 and L2 Jet-Based Trigger Efficiencies			
Channel	Level 1	Level 2	Total
$WH \to e\nu b\bar{b}$	0.973	0.97	0.94
$WH \to \mu\nu b\bar{b}$	0.902	0.98	0.89
$WH \to \tau\nu b\bar{b}$	0.930	0.96	0.90
$ZH \to eeb\bar{b}$	0.993	0.98	0.98
$ZH \to \mu\mu b\bar{b}$	0.943	0.99	0.94
$ZH \to \nu\nu b\bar{b}$	0.938	0.94	0.90

Table 4: Level 1 trigger efficiencies for associated Higgs boson production channels. The efficiencies are based on Monte Carlo. The efficiencies are measured after first requiring two 8 GeV off-line jets.

3.3 Event Samples

To study the selection efficiencies of signal events, we used Monte Carlo (MC) samples generated using `PYTHIA`. Background events were generated using `COMPHEP`, `ALPGEN`, `ONETOP`, `VECBOS`, and `PYTHIA`. In the cases of `COMPHEP` and `ONETOP`, `PYTHIA` was used to simulate fragmentation. For all events, generation was followed by a full hit-based `GEANT` simulation of the Run IIA DØ detector. All events were then reconstructed using the current version of the DØ reconstruction software (p13.06.01).

For this study, select processes were simulated including a Poisson-distributed minimum bias (mb) overlay with an average of 5.0 events. The 5.0 mb inclusion is intended to simulate the high luminosity environment of Run IIB at the Tevatron with an average luminosity of $\mathcal{L} \approx 2 \times 10^{32} cm^{-2} \cdot s^{-1}$ and were produced with `PYTHIA`.

3.4 Event Selection

Selection begins with choosing well-reconstructed physics objects in the events. Standard DØ object-ID criteria were applied to these objects. Furthermore, η and p_T acceptance cuts were applied. These cuts are listed in Table 5. Upon selection of the physics objects to be used in the event, selection quantities were derived and utilized.

The selection procedure is as follows:

Object	$\|\eta\|$ Cut	p_T Cut (GeV/c)
Electron	2.4	5.0
Muon	2.0	5.0
Jet	2.5	15.0

Table 5: Acceptances used for physics objects.

- Events with isolated leptons are given an event weight determined by the probability that the lepton would not be identified, as described in Section 3.6.1. A lepton is considered isolated if it has an angular separation from all jets of at least $\Delta R > 0.5$ and $p_T > 8$ GeV/c.
- Next, a cut is placed on the missing transverse energy. The $\not\!\!E_{\rm T}$ was corrected for jet energy scale (JES) corrections and for all the muons in the event. The cut was placed to accept all events with at least 25 GeV of $\not\!\!E_T$.
- The $\not\!\!E_{\rm T}$ significance is required to be at least 4.5. This cut is designed primarily to reduce the QCD background. A description of how this variable is calculated can be found in [8].
- After the $\not\!\!E_{\rm T}$ significance cut, a cut is placed on the minimum difference in ϕ between the $\not\!\!E_T$ direction and any jet in the event. This cut removes any events with $\Delta\phi(\not\!\!E_{\rm T}, jets) < 0.15$.
- The event is required to contain two or more $R = 0.5$ cone jets with at least 15 GeV/c of p_T.
- The two leading jets in p_T were given an event weight based on the Run IIB b-tagging parameterizations described in Section 3.6.1. The leading jet in p_T was evaluated using the "tight" b-tagging parameterization and the second leading jet was evaluated using the "loose" parameterization.
- A cut is placed on the p_T of the b-tagged jet candidates. This cut was set to accept jets with $p_T > 20$ GeV/c.
- Events with a fourth jet over 22.5 GeV/c in p_T are vetoed.
- Next, a cut is placed on the H_T in the event. This variable is calculated as the scalar p_T sum of all jets in the event passing JET-ID cuts. For jets which contain a muon, the p_T of the jet-muon system is used in the sum. This cut was placed to remove all events with H_T larger than 200 GeV/c.

After performing standard selection requirements on the event, many backgrounds remain large compared to the signal expectation. In order to further distinguish between signal and background events, one can attempt to create a useful selection variable using other variables with limited discrimination power. One means of creating such a selection variable is the use

of neural network techniques. This technique essentially combines the discrimination power of several variables to form a single variable with a greater ability to separate signal and background than any of the input variables alone. After the basic selection procedure, the largest remaining backgrounds are $t\bar{t}$ and $W/Zb\bar{b}$. It is these backgrounds which we attempt to remove by using neural networks.

The neural network selection is performed after the standard event selection. The final steps of the selection procedure consist of the following:

- A cut was placed on the $t\bar{t}$ neural network (NN) value, optimized for each generated Higgs boson mass. The variables of the NN are described in Section 3.5, and the optimized cut values are given in Table 11.
- After performing the above selection, there was no distinguishing power left in the $W/Zb\bar{b}$ NN (described in Section 3.5). As such, no cut was placed on this value.
- A window cut was placed on the reconstructed $b\bar{b}$ mass, optimized for a 10% dijet mass resolution for each generated Higgs mass. The optimized cut values are given in Table 11. This cut was placed only for the purposes of making a comparison to the reported SHWG analysis values.

3.5 Neural Networks

To discriminate against the large contribution of $t\bar{t}$ and single top events with a similar topology to the ZH signal, a NN was trained to eliminate these events. The inputs to the $t\bar{t}$ NN are as follows:

- H_T
- The largest p_T of any untagged jets
- The aplanarity of the n-jet system
- The net p_T imbalance of the $\not\!\!E_T - b\bar{b}$ system
- The first four transverse-modified Fox-Wolfram (FW) moments

A full description of the FW moments can be found in [9]. An $8 \times 16 \times 1$ NN was generated and trained using ZH signal and $t\bar{t} \to \ell\nu bjj\bar{b}$ events. Figure 6 shows the output of the $t\bar{t}$ NN for ZH signal and $t\bar{t}$ background events. The $t\bar{t}$ NN training was performed after requiring 2 b-tagged jets and $H_T < 225$ GeV/c.

To isolate $W/Zb\bar{b}$ events from ZH signal events, a NN was created with the following inputs:

- H_T
- Leading jet p_T
- Second to leading jet p_T

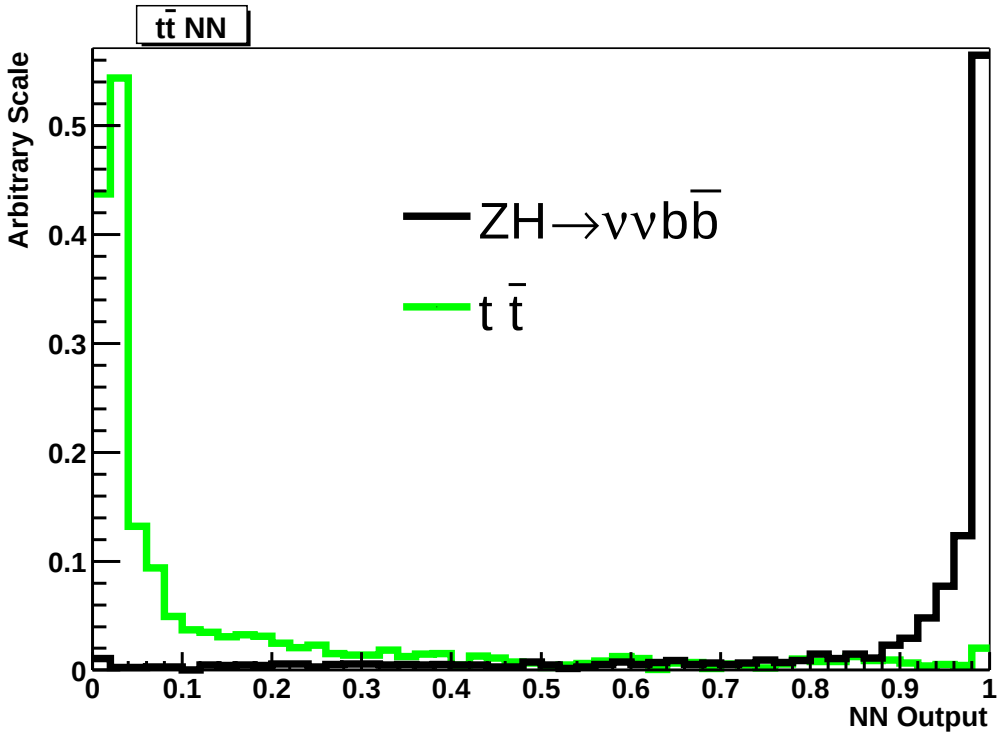

Figure 6: Output of the $t\bar{t}$ NN for signal and $t\bar{t}$ events.

- The angle between the leading jet and the jet-jet system
- The acoplanarity of the jet-jet system
- ΔR between the tagged jets

A $6 \times 12 \times 1$ NN was generated and trained using ZH signal and $Wb\bar{b}$ events. Figure 7 shows the output of the $Wb\bar{b}$ NN for ZH signal and $Wb\bar{b}$ background events. The $W/Zb\bar{b}$ NN training was performed after requiring 2 b-tagged jets and $H_T < 225$ GeV/c.

All neural networks used in this analysis were created and trained using the Stuttgart Neural Network Simulator package [10]. During training, the `RPROP` method of node-weight adjustment was used. The `RPROP` method is similar to the standard back-propagation method, but is considerably faster. Furthermore, all networks were designed with an output of zero for background and one for signal.

3.6 b-jet Tagging and Mis-tag Rates

The reduction of light-quark background events relies on being able to identify the relatively long-lived b-quark decays. In order to determine the rates of b-quark tagging and light quark mis-tagging, the performance of the Run IIB silicon detector is evaluated. Detailed studies of b-quark tagging in Run IIB are outlined in [11].

Based on the study of b-tagging performance (b-tagging efficiency versus mis-tagging rate) in Run IIB, the operating point of the b-tagging algorithm was chosen to provide 62%

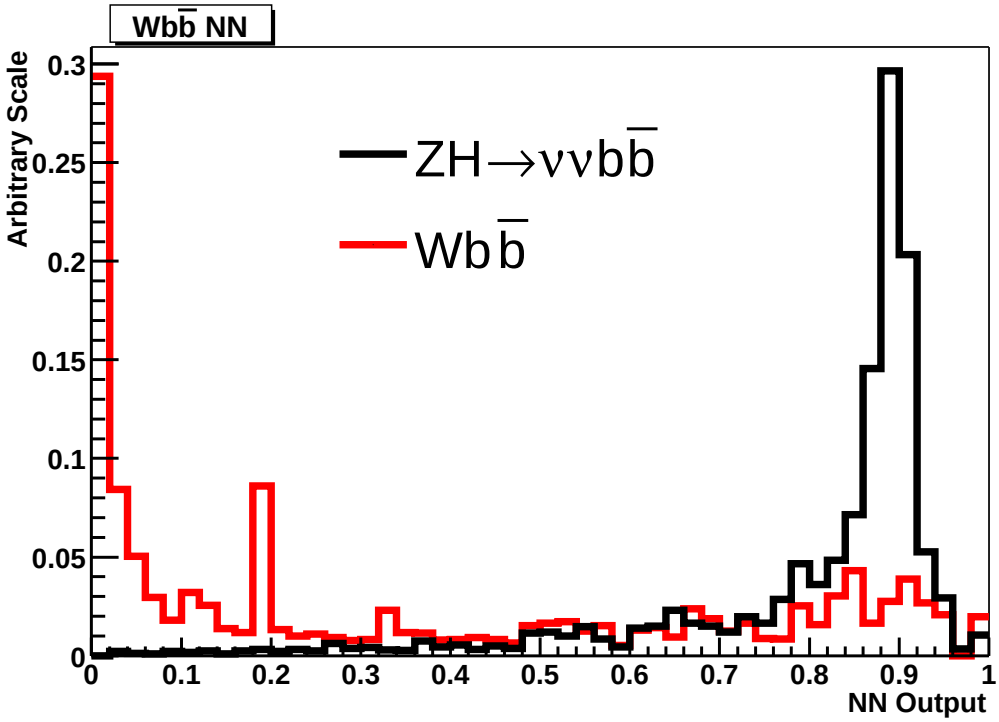

Figure 7: Output of the $W/Zb\bar{b}$ NN for signal and $Wb\bar{b}$ events.

b-tagging efficiency per b jet and 0.8% mis-tagging rate per light quark jet at the design luminosity. The b-tagging efficiency and mis-tag rate are shown in Figure 8 as functions of jet η and E_T.

Comparisons of b-tagging performance in Run IIA and Run IIB prior to making any analysis-specific cuts show significant improvement in the expected double tagging rate for signal events even at luminosities much higher than in Run IIA (see Table 6).

	$P(n_b \geq 1)$	$P(n_b \geq 2)$
WH + 0 mb in Run IIA	70.7 ± 1.4	23.4 ± 0.8
ZH + 5 mb in Run IIB	76.9 ± 1.0	32.0 ± 1.1

Table 6: Probability to tag an event with at least 1 and greater than 1 b-jets in the final state in Run IIA and Run IIB. The WH Monte Carlo was simulated with 0 additional interactions (0 mb) while the ZH Monte Carlo was simulated with the equivalent of 5 additional interactions.

An additional gain of at least 4% can be obtained by using an alternate b-tagging method based on soft lepton tagging, but for the price of higher mis-tagging rate. However, soft lepton tagging is not included in this study.

Since most of background channels were simulated with the present Run IIA geometry, it is impossible to apply any b-tagging procedure directly to the background samples. Instead,

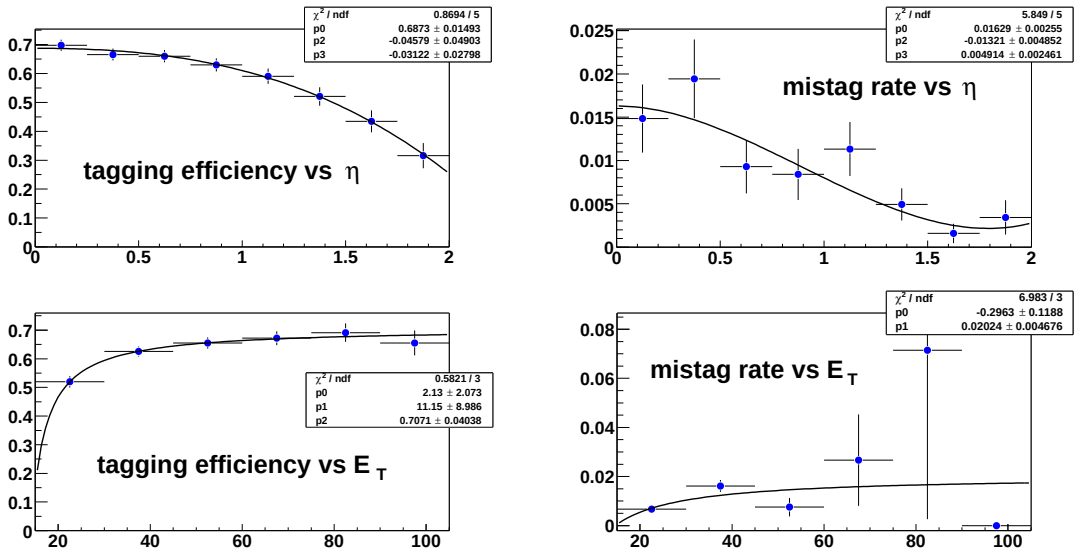

Figure 8: b-tagging efficiency (left) and mis-tagging rate (right) in Run IIB.

one can use both b-tagging and mis-tagging rates parameterized as functions of jet p_T and η. These parameterizations are shown in Figures 8 and 9.

3.6.1 Run II Silicon Detector Upgrade Parameterizations

The procedure used to apply the Run IIB parameterizations is as follows. For b-tagging, the two highest-p_T jets are considered b quark candidates and are weighted depending on their flavor. Jets originating from b quarks (based on generator information) are weighted with the 2-d (η, p_T) signal tagging parameterization (P_{b-tag}). Jets originating from c quarks are weighted with the signal tagging parameterization divided by 3 ($P_{b-tag}/3$). Jets originating from light quarks are weighted with the mis-tag parameterization ($P_{mis-tag}$). For each additional jet above 15 GeV/c in p_T, an additional weighting factor of $1 - P_i$ is multiplied based on the flavor of the jet. If either of the two highest p_T jets has $p_T < 20$ GeV/c, the event weight is 0. To be more explicit, the procedure for inclusive b-jet events is shown in the following examples (assuming the p_T requirements for the jets are satisfied):

- 2 b-jets: Weight = $P_{b-tag1} \times P_{b-tag2}$
- 1 b-jet, 1 light quark jet: Weight = $P_{b-tag1} \times P_{mis-tag1}$
- 2 b-jets, 1 light quark jet: Weight = $P_{b-tag1} \times P_{b-tag2} \times (1 - P_{mis-tag1})$

For events including only light quark jets, the weighting for each event is done as follows:

- 2 jets: Weight = $P_{mis-tag1} \times P_{mis-tag2}$
- 3 jets: Weight = $P_{mis-tag1} \times P_{mis-tag2} \times (1 - P_{mis-tag3}) + P_{mis-tag1} \times P_{mis-tag3} \times (1 - P_{mis-tag2}) + P_{mis-tag2} \times P_{mis-tag3} \times (1 - P_{mis-tag1})$

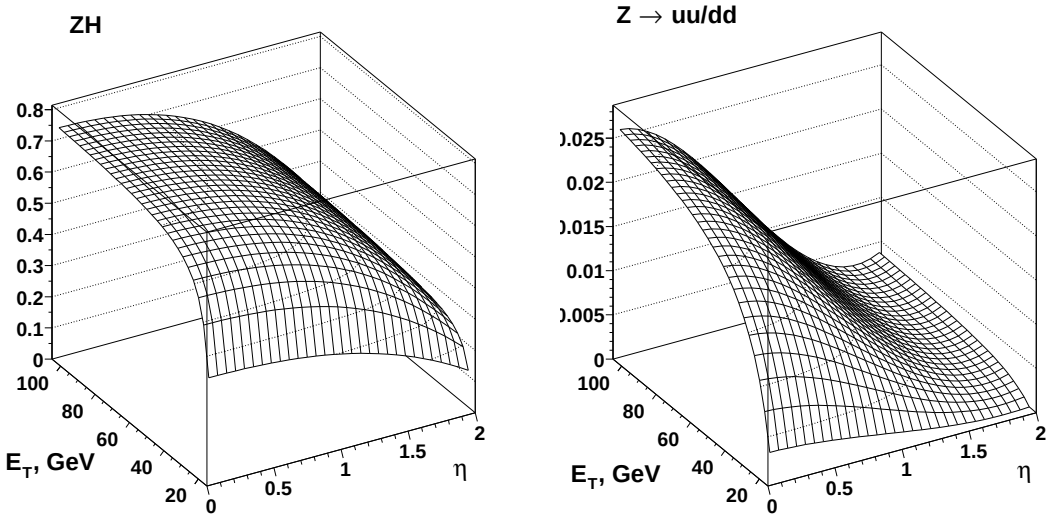

Figure 9: Parameterized b-tagging efficiency (left) and mis-tagging rate (right) in Run IIB.

- 4 jets: Weight = $P_{mis-tag1} \times P_{mis-tag2} \times (1 - P_{mis-tag3}) \times (1 - P_{mis-tag4}) + P_{mis-tag1} \times P_{mis-tag3} \times (1 - P_{mis-tag2}) \times (1 - P_{mis-tag4}) + P_{mis-tag1} \times P_{mis-tag4} \times (1 - P_{mis-tag2}) \times (1 - P_{mis-tag3}) + P_{mis-tag2} \times P_{mis-tag3} \times (1 - P_{mis-tag1}) \times (1 - P_{mis-tag4}) + P_{mis-tag2} \times P_{mis-tag4} \times (1 - P_{mis-tag1}) \times (1 - P_{mis-tag3}) + P_{mis-tag3} \times P_{mis-tag4} \times (1 - P_{mis-tag1}) \times (1 - P_{mis-tag2})$

For high-p_T leptons, a similar procedure is used. Leptons are obtained from the generator list. No energy or p_T smearing is performed. All leptons (e, μ only) within the constraints given in Table 5 are considered. We accept events that have leptons that are not identified because either the leptons fail the isolation criteria or they fail to be reconstructed, where the probability to reconstruct a lepton is given by P_{reco}. A lepton is considered isolated if it has an angular separation from all jets of at least $\Delta R > 0.5$ and $p_T > 8$ GeV/c. If the lepton satisfies the isolation criteria, the event is given an additional weighting factor of $(1 - P_{reco})$.

3.7 Dijet Mass Resolution

A dijet mass resolution of 10% is chosen as the operating point for this analysis, based on studies described in Section 5. To obtain this point, the reconstructed dijet mass width is rescaled to this resolution (retaining the original shape). The scaling was performed for all Higgs boson signal Monte Carlo events as well as WZ and ZZ Monte Carlo in which the tagged jets originated with a b quark. In the case of Higgs signal events, the mass was rescaled relative to the mass of the generated Higgs boson. For WZ and ZZ events, the mass was rescaled relative to 91.2 GeV/c^2. Figures 10 and 11 show the original and rescaled masses for $ZH \to \nu\nu b\bar{b}$ events and WZ/ZZ events, respectively.

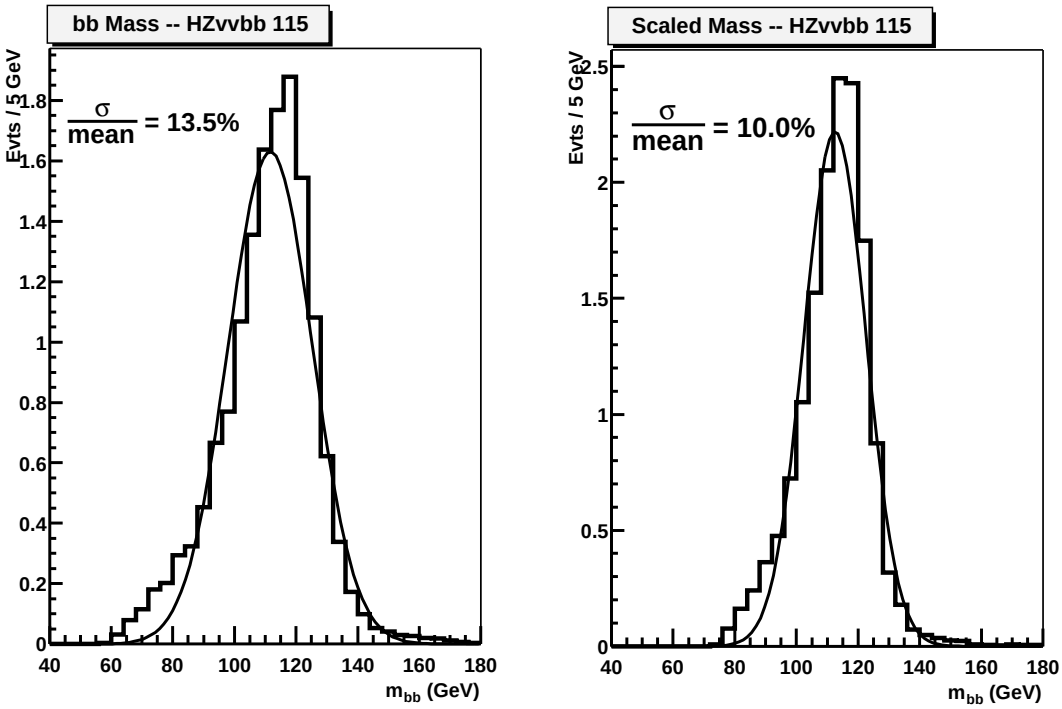

Figure 10: Original and rescaled $b\bar{b}$ masses for ZH signal Monte Carlo events.

3.8 Evaluation of QCD Backgrounds

The SHWG report made an estimate of the QCD background to the $ZH \rightarrow \nu\nu b\bar{b}$ signal based on conjectural arguments. In that study, the QCD background rate was taken to be 50% of the total inclusive background and no determination was made of the actual rate. In this study, we endeavor to improve this projection by making an actual measurement of this process. To do so, we will use a Run IIA data sample to count the number of events passing the selection process. However, we cannot make a proper measurement using this data sample alone. At this time, we do not understand the trigger rates in Run IIA well enough to make a luminosity determination. To fix this, we will normalize the luminosity of our data sample to a Run I data sample in which the luminosity was well-measured. Also, although we assume our data sample to be predominantly QCD multi-jet production with a small number of non-QCD events, we do not know the b quark content of the data. To find this value, we rely on generated Monte Carlo events to measure the ratio of cross section acceptance for light quark QCD events and $b\bar{b}$ QCD events. Finally, the b-tagging in the data sample does not match that which we used for our Monte Carlo study. As such, we will determine the b-tagging efficiency in the data by using the Run IIB b-tagging parameterizations.

To evaluate the expected contribution from QCD backgrounds, we begin by counting the number of events which pass the full selection procedure of the $ZH \rightarrow \nu\nu b\bar{b}$ analysis. Upon selecting a number of events from the data sample (N_{select}), we need to determine the number of events we expect in a given amount of luminosity ($N(\mathcal{L}_{given})$). First, the luminosity of the data sample is determined ($\mathcal{L}_{measured}$) by a comparison to the Run I data sample. Next,

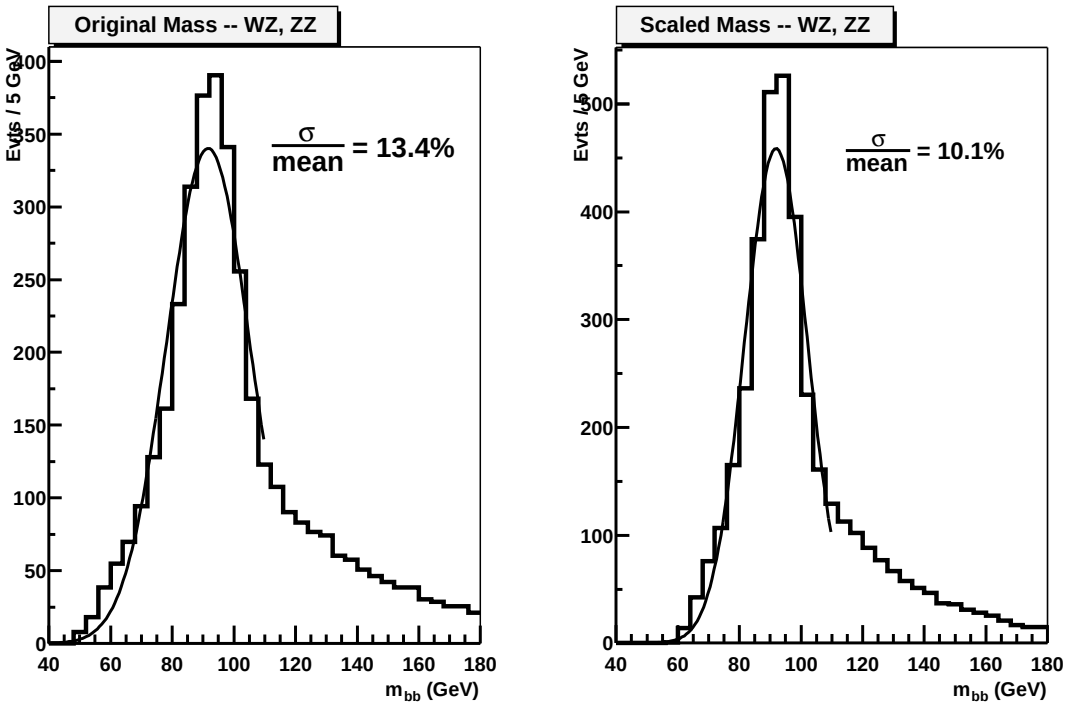

Figure 11: Original and rescaled $b\bar{b}$ masses for WZ/ZZ Monte Carlo events.

we calculate the cross section ratio of light quark QCD Monte Carlo events accepted to $b\bar{b}$ QCD Monte Carlo events accepted (R_{accept}). Next we evaluate the b-tagging efficiency (ϵ_{tag}) in the data sample using the Run IIB tagging method. The calculation of the number of events expected in a given amount of luminosity, $\mathcal{L}_{given}$, is shown in Equation 1:

$$N(\mathcal{L}_{given}) = N_{select} \times R_{accept} \times \epsilon_{tag} \times \mathcal{L}_{given}/\mathcal{L}_{measured} \quad . \tag{1}$$

The Run IIA data sample consists of events containing at least one good jet with at least 10 GeV/c in p_T and satisfying a muon trigger. The muon trigger provides an adequate data sample and is used in this study in place of a pure $\not\!\!E_T$ trigger. For this sample, all bad calorimeter and bad muon runs were removed. The reconstruction and use of all physics objects is the same as that used for the Monte Carlo. To avoid bias from the muon trigger, we eliminate all events with high p_T muons.

We first evaluate the integrated luminosity of this sample by making a comparison to a Run I $\not\!\!E_T$ + jets study [12]. To normalize our luminosity to that found in this study, we reproduce their cuts in our data sample:

- p_T, leading jet > 25 GeV/c
- p_T, second-to-leading jet > 10 GeV/c
- $\not\!\!E_T > 25$ GeV
- $\Delta\phi(\not\!\!E_T, jets)_{min} > 0.25$

Using the above cuts, the Run I study found 399,557 events in 85.2±3.7 pb^{-1}. Performing this selection on the Run IIA data sample, we find 40,184 events, which normalizes to 8.6 ± 0.4 pb^{-1}.

To evaluate the $b\bar{b}$ content of this sample, we use Monte Carlo samples generated by PYTHIA for light quark QCD and direct $b\bar{b}$ QCD production. The generator cross section is 35 μb for the light quark QCD sample and 0.1 μb for the $b\bar{b}$ QCD sample. Here, we use a set of selection cuts that more closely resembles the set of cuts that will be used in the analysis:

- p_T, 2 leading jets > 20 GeV/c
- $\not\!\!E_T > 25$ GeV
- $H_T < 200$ GeV/c

We do not incorporate the full analysis selection for this step as we need to keep a sufficient amount of statistics to make a reliable determination of rates. For example, requiring two b-tagged jets would leave no events in the light quark QCD Monte Carlo sample. With this set of cuts, we find an acceptance of 0.26% for the light quark QCD Monte Carlo sample and 0.57% for the $b\bar{b}$ QCD Monte Carlo sample. Using these acceptances and the Monte Carlo cross sections, we find a ratio of $R_{accept} = 1/160$ for the relative accepted cross sections. As the $b\bar{b}$ QCD Monte Carlo sample only includes direct $b\bar{b}$ production and likely has an underestimated Monte Carlo cross section, a more conservative number is a ratio of $R_{accept} = 1/100$.

As the data sample uses tracking and b-tagging efficiencies which differ greatly from what is being used in this study, we cannot use the b-tagging performance directly from the data sample. However, as we must have an estimate of the actual b-tagging rate for this sample, we evaluate the b-tagging efficiency using parameterizations for the Run IIB b-tagging [11]. To do so, we use the Run IIA data sample again. We consider the two highest p_T jets in the event to be b-quark candidates and weight them according to their probability to be tagged as described in Section 3.6.1. The sample consists of 934,113 events. After requiring two b-tagged jets, the remaining sample was 92,357 events. This results in a double-tagging efficiency of $\epsilon_{tag} = 9.9\%$. The fake double-tag rate for this sample can be measured using the Run IIB mis-tagging parameterizations. Here we find a fake double tag rate of $\epsilon_{faketag} = 1.1 \times 10^{-4}\%$. This faked tag rate correpsonds to a light quark QCD expectation of less than 0.1 events per fb^{-1}.

Finally, to evaluate the expected number of events in the analysis samples, we begin by counting the number of events which pass the full selection, N_{select}, in the Run IIA data sample. Once the number of selected events is found, we multiply by the ratio of accepted cross sections to obtain the expected number of b-quark events. Next, we multiply by the double-tagging efficiency to determine the number of expected events. We can normalize this number to an appropriate amount of integrated luminosity by scaling the measured amount of luminosity in our data sample. The procedure to determine the expected number of events in 1 fb^{-1} is outlined in Equation 2:

$$N(1\ fb^{-1}) = N_{select} \times R_{accept} \times \epsilon_{tag} \times 1\ fb^{-1} \times 1/8.6\ pb^{-1} = 0.115 \times N_{select}. \qquad (2)$$

3.9 Results

The selection efficiencies for signal and background Monte Carlo are shown in Tables 7, 8, 9 and 10. These efficiencies are sequential and are evaluated using the Run IIB b-tagging and lepton-ID parameterizations. The expected number of signal and background events in 1 fb^{-1} are also shown.

Higgs Mass (GeV/c^2)	115	120	130
Cross Section (pb)	0.108	0.094	0.071
Branching Ratio	0.732×0.20	0.679×0.20	0.527×0.20
Lepton Veto	98.9	99.1	99.3
$\not\!\!E_{\rm T} > 25\,{\rm GeV}$	87.3	87.6	89.2
$\not\!\!E_{\rm T}$ Signif > 4.5	92.5	92.9	93.2
$\Delta\phi(jets, \not\!\!E_{\rm T}) > 0.15$	90.8	90.6	91.4
Jet Selection	83.4	84.4	87.1
b-Tagging	41.0	40.9	41.8
Jet p_T Cuts	97.4	97.3	97.9
4^{th} Jet Veto	95.9	96.5	95.7
H_T Cut	88.7	87.8	86.5
NN Cut	83.4	83.8	85.7
Mass Window	91.8	92.9	93.1
Acceptance	15.7	16.2	17.8
Trigger Efficiency	90.0	90.0	90.0
Events in 1 fb^{-1}(w/o MW)	2.44	1.99	1.29
Events in 1 fb^{-1}	2.24	1.85	1.20

Table 7: Selection efficiencies (%) for $ZH \to \nu\bar{\nu}b\bar{b}$ for m_H =115, 120 and 130 GeV/c^2 and expected numbers of events in 1 fb^{-1} with and without mass window (MW). The branching ratio is the product of BR($H \to b\bar{b}$) multiplied by BR($Z \to \nu\bar{\nu}$).

The following important observations are evident from the selection efficiencies in Tables 7, 8, 9 and 10:

- The lepton veto has high finding efficiencies of 75%, 65% and 15% for WH events with e, μ and τ leptons, respectively. Events that are vetoed are subject to analysis by $WH \to \ell\nu b\bar{b}$ and $ZH \to \ell\ell b\bar{b}$ search channels.

- The b-tagging efficiencies are evaluated after missing transverse energy and Jet Selection cuts, but before $t\bar{t}$ rejection cuts are applied. This is to avoid biases in the p_T distribution of the b jets in comparison with the $\ell\nu b\bar{b}$ search channel. These efficiencies are approximately 41% for ZH signal events, 19% for $Wb\bar{b}$ background and 38% for $t\bar{t}$ events.

- The NN selection cut is the single-most powerful step in the analysis keeping approximately 84% of the ZH signal while retaining only 15% of the $t\bar{t}$ events.

Process	$ZH \to ee b\bar{b}$	$ZH \to \mu\mu b\bar{b}$	$ZH \to \tau\tau b\bar{b}$
Cross Section (pb)	0.108	0.108	0.108
Branching Ratio	0.732×0.03	0.732×0.03	0.732×0.03
Lepton Veto	19.2	16.7	69.2
$\not\!\!E_{\rm T} > 25\,{\rm GeV}$	20.8	63.4	55.9
$\not\!\!E_{\rm T}$ Signif > 4.5	42.2	81.6	62.4
$\Delta\phi(jets, \not\!\!E_{\rm T}) > 0.15$	75.5	90.3	74.7
Jet Selection	82.0	87.1	95.1
b-Tagging	38.2	42.2	37.0
Jet p_T Cuts	95.3	97.1	94.2
4^{th} Jet Veto	85.2	92.3	79.4
H_T Cut	81.4	89.3	72.7
NN Cut	68.2	75.7	36.2
Mass Window	82.3	84.6	83.5
Acceptance	0.15	1.47	1.05
Trigger Efficiency	98.0	94.0	92.0
Events in 1 fb^{-1}(w/o MW)	0.005	0.05	0.04
Events in 1 fb^{-1}	0.004	0.04	0.03

Table 8: Selection efficiencies (%) for charged lepton ZH events with m_H =115 GeV/c^2 and expected numbers of events in 1 fb^{-1} with and without mass window (MW). The branching ratio is the product of BR($H \to b\bar{b}$) multiplied by BR($Z \to$e$^+$e$^-$), similarly for μ and τ decays of the Z boson.

3.9.1 Optimization Procedures

The specific reconstructed $b\bar{b}$ mass and NN cuts are chosen to maximize the significance of the search. To do so, the $S/\sqrt{B}$ value was scanned as a function of each variable to find the maximal value. The optimization was done for a reconstructed $b\bar{b}$ mass resolution of 10%. An example of this process is shown in Figures 12 and 13 for the reconstructed $b\bar{b}$ mass using m_H = 115 GeV/c^2. The optimized selection values for the $b\bar{b}$ mass and $t\bar{t}$ NN chosen for each generated Higgs mass are shown in Table 11.

Process	$WH \to e\nu b\bar{b}$	$WH \to \mu\nu b\bar{b}$	$WH \to \tau\nu b\bar{b}$
Cross Section (pb)	0.186	0.186	0.186
Branching Ratio	0.732×0.11	0.732×0.11	0.732×0.11
Lepton Veto	25.4	35.0	84.7
$\not\!\!E_{\rm T} > 25\,{\rm GeV}$	79.4	87.1	80.0
$\not\!\!E_{\rm T}$ Signif > 4.5	91.4	91.2	85.8
$\Delta\phi(jets, \not\!\!E_{\rm T}) > 0.15$	93.8	88.3	88.0
Jet Selection	81.9	89.8	90.3
b-Tagging	37.5	39.3	37.6
Jet p_T Cuts	95.5	94.4	95.3
4^{th} Jet Veto	96.2	92.6	89.8
H_T Cut	92.9	82.3	81.7
NN Cut	62.2	65.5	50.4
Mass Window	79.3	83.3	87.0
Acceptance	2.23	3.43	5.33
Trigger Efficiency	95.0	90.0	90.0
Events in 1 fb^{-1}(w/o MW)	0.39	0.54	0.80
Events in 1 fb^{-1}	0.31	0.45	0.70

Table 9: Selection efficiencies (%) for leptonic WH events with m_H =115 GeV/c^2 and expected numbers of events in 1 fb^{-1} with and without mass window (MW). The branching ratio is the product of BR($H \to b\bar{b}$) multiplied by BR($W \to$eν), similarly for μ and τ decays of the W boson.

Background Source	$Wb\bar{b}$	$Zb\bar{b}$	$t\bar{t}(\ell\nu jj/\ell\nu\ell\nu)$	$t(W^*)$	$t(Wg)$	WZ	ZZ	QCD
Cross Section (pb)	10.6	4.47	7.00	0.80	2.26	3.20	1.70	
Branching Ratio	0.21*	0.20	0.29*/0.10	0.21*	0.21*	1.00	1.00	
# MC Events	123k		65k/56k	29k	60k	37k	78k	
Lepton Veto	28.6		32.2/26.6	29.6	25.6	77.3	82.1	
$\not\!\!E_{\rm T} > 25\,{\rm GeV}$	64.1		90.5/92.7	91.1	87.9	32.5	34.9	
$\not\!\!E_{\rm T}$ Signif > 4.5	93.3		84.7/90.2	90.6	94.8	82.7	79.3	
$\Delta\phi(jets, \not\!\!E_{\rm T}) > 0.15$	92.3		91.2/87.2	93.3	95.5	92.1	93.7	
Jet Selection	25.4		99.2/95.4	92.9	67.5	69.1	70.1	
b-Tagging	19.2		36.6/36.2	26.3	10.7	3.55	7.97	
Jet p_T Cuts	89.2		95.8/97.2	96.5	85.6	91.3	96.8	
4^{th} Jet Veto	96.6		43.2/70.9	84.8	86.1	89.3	94.6	
H_T Cut	92.3		38.3/54.2	61.2	81.1	94.0	95.0	
NN Cut	63.2		10.8/26.0	41.2	33.8	48.6	73.1	
Mass Window	14.6		31.3/19.3	21.5	21.5	20.2	14.0	
Acceptance	0.057		0.044/0.13	0.25	0.064	0.035	0.106	
Trigger Efficiency	90.0		90.0/90.0	90.0	90.0	90.0	90.0	
Events from e, μ	1.17		0.81/0.81	0.40	0.29	1.01	1.61	
Events from τ	0.91		0.63/incl.	0.31	0.23	incl.	incl.	
Events in 1 fb^{-1}								
(w/o MW)	14.2	8.08	8.80	3.30	2.42	5.00	11.5	61.2
(w/ MW)	2.08	1.18	2.24	0.71	0.52	1.01	1.61	10.2

Table 10: Selection efficiencies (%) for significant background processes to the $ZH \to \nu\bar{\nu}b\bar{b}$ search and expected numbers of events in 1 fb^{-1} with and without mass window (MW). These values are obtained using the $m_H = 115$ GeV/c^2 optimization points. The branching ratio corresponds to the relevant leptonic decay modes of the W and Z bosons. *The number of τ events is evaluated separately and included at the bottom of the table.

m_H (GeV/c^2)	Mass Window	$t\bar{t}$ NN
105	92 - 128	0.70
115	100 - 136	0.75
120	104 - 140	0.73
125	112 - 148	0.75
130	114 - 150	0.77

Table 11: Optimized selection cuts for $ZH \to \nu\bar{\nu}b\bar{b}$ signal Monte Carlo.

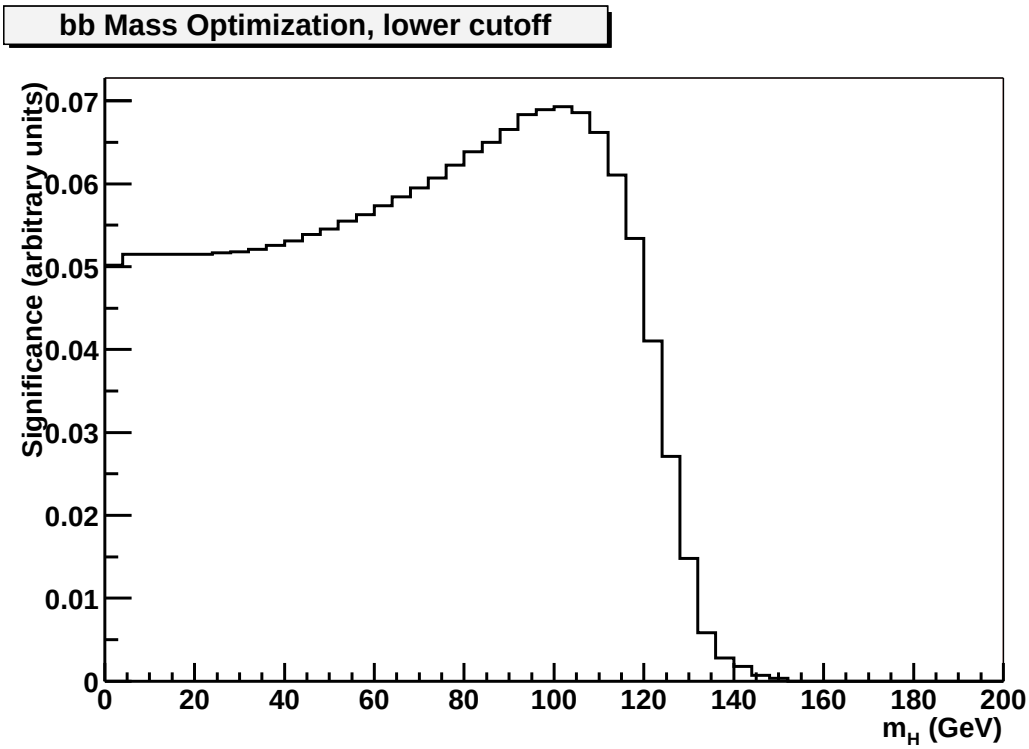

Figure 12: $S/\sqrt{B}$ scan for a lower mass cut, $m_H = 115$ GeV/c^2.

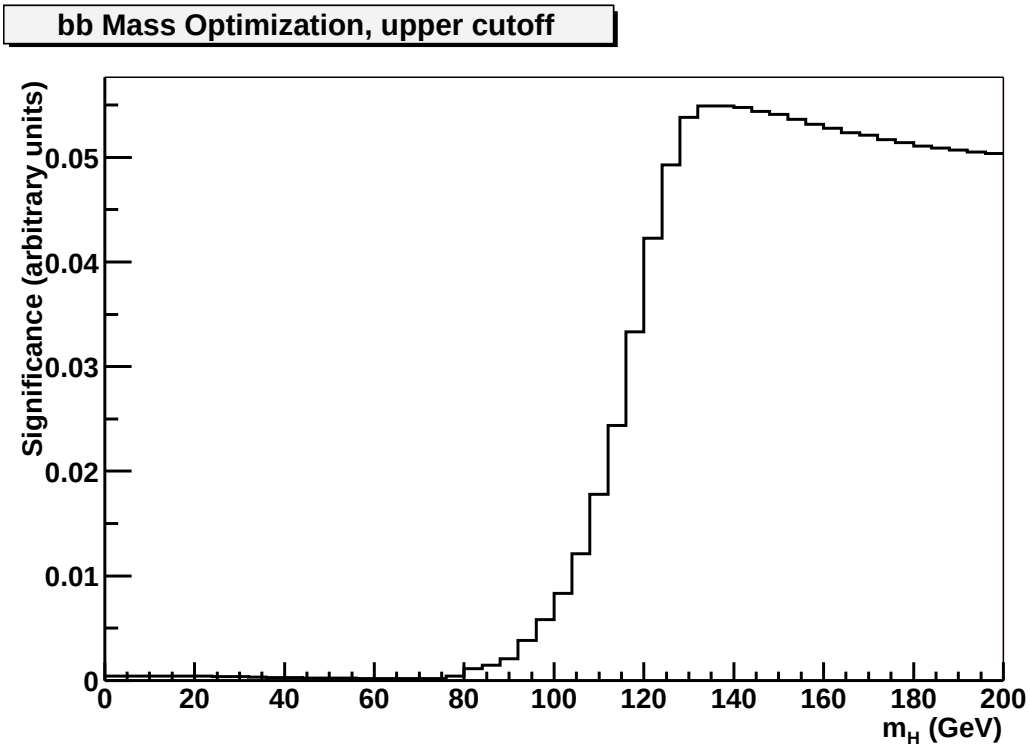

Figure 13: $S/\sqrt{B}$ scan for an upper mass cut, $m_H = 115$ GeV/c^2.

4 Study of Neural Network Improvements

In this document, we are combining two analyses which use different detector simulations, reconstruction algorithms, and Monte Carlo samples. It is therefore necessary to ensure the reproducibility of results by the two experiments for each analysis technique and, in particular, the neural network improvements. To this end, the full $WH \to \ell\nu b\bar{b}$ analysis was reproduced with the DØ analysis framework used for the $ZH \to \nu\nu b\bar{b}$ analysis. This exercise reinforces our understanding of common background sources and the analysis techniques used. Furthermore, the task remains to determine the neural network scale factors to apply to the CDF $WH \to \ell\nu b\bar{b}$ analysis when making the full combination, described in Section 6. The scale factor of 1.6 (effective luminosity) was obtained from a Run I CDF Higgs search. This choice agrees well with the NN improvements in the SHWG $WH \to \ell\nu b\bar{b}$ analysis and also the current DØ $ZH \to \nu\nu b\bar{b}$ analysis. However, in this section we will determine the individual efficiency factors for the signal and each background source.

4.1 Reproduction of CDF WH Results

The first step in this process is to reproduce the salient features of the CDF WH analysis. To do this, the selection steps used in the $WH \to \ell\nu b\bar{b}$ analysis were repeated with a few minor modifications. The event selection was performed as follows:

- 1 electron or muon with $p_T > 20\,\mathrm{GeV}/c$
- $\not\!\!E_{\mathrm{T}} > 20\,\mathrm{GeV}$ (corrected)
- Remove $Z \to \ell^+\ell^-, \ell = e, \mu$
  - Includes $76 < M_{\ell\ell} < 106\,\mathrm{GeV}/c^2$
- Jet Requirements: 2 or 3 Tight Jets
  - Tight Jets: $E_T > 10$ GeV $|\eta| < 2.0$ (corrected, cone= 0.5)
  - Loose Jets: $E_T > 10$ GeV $|\eta| < 2.4$ (corrected, cone= 0.5)
- Additional Kinematic Cuts
  - One Tight Jet with $E_T > 24\,\mathrm{GeV}$
  - No Third Jet with $E_T > 22\,\mathrm{GeV}$
  - No isolated track with $p_T > 12\,\mathrm{GeV}/c$
- Require 2 b-tagged jets
- Window cut on the reconstructed dijet mass at $100 < m_{b\bar{b}} < 136$ GeV$/c^2$

The changes in selection procedures were made to adapt the process to the DØ event reconstruction. Initially, we did not include isolated tracks in the lepton identification step. Jet energy scale (JES) corrections are propagated back to the $\not\!\!E_{\mathrm{T}}$. We use JES-corrected,

$R = 0.5$ cone jets, while the CDF analysis used uncorrected $R = 0.4$ cone jets. This difference in jet treatment impacts the transverse energy requirements for jets in the kinematic selection. To account for this, changes were made in the kinematic selection to match the efficiencies for WH signal Monte Carlo found by the CDF WH analysis. Also, the veto on 2 or more leptons in the event was withdrawn from the first selection step. This was done because we observed no change in efficiency for a second lepton veto after the Z veto and the isolated track veto of the kinematic cuts. As we were unable to directly apply the CDF b-tagging procedure, b-tagging was performed using the DØ Run IIB double tagging parameterizations as described in Section 3.6.1. Finally, the mass window was applied with the assumption of 10% dijet mass resolution and the Monte Carlo events were scaled as described in Section 3.7.

For this exercise, we used $m_H = 115$ GeV/c^2 signal Monte Carlo to evaluate signal efficiencies. For background, we used the same samples as were used in the ZH analysis. To evaluate the number of expected events for each Monte Carlo sample, the trigger efficiencies from the CDF analysis are used. The one exception is that of the $Wb\bar{b}$ background, as CDF normalized their result to data. In this case, we used the same $Wb\bar{b}$ Monte Carlo sample as used in the $ZH \to \nu\nu b\bar{b}$ analysis, which has a generator cross section of 10.6 pb. Furthermore, we included the cross-efficiencies from $ZH \to \ell\ell b\bar{b}$ signal Monte Carlo and also that of an inclusive ZZ background Monte Carlo sample.

The relative efficiencies for each selection step are shown in Tables 13-15. The efficiencies can be compared to those obtained in the CDF WH analysis and shown in Tables 1-2. There is good agreement in general for both signal and background. Table 16 shows an expected $S/\sqrt{B}$ value of 0.55 for the DØ WH analysis.

Although this result is different from the value of $S/\sqrt{B} = 0.45$ obtained by the CDF WH analysis for the $m_H = 115$ GeV/c^2 mass point, the increase can be accounted for. First, the lepton ID efficiency used in this analysis is 8% more efficient than that found in the CDF WH analysis. Second, we observe an increase in double b-tagging efficiency of 14% (from 28% to 31.5%) by using the DØ Run IIB tagging parameterizations. This increase in tagging efficiency has been independently confirmed by using the DØ Run IIB tagging parameterizations in the CDF analysis framework. Additionally, the $100 < m_H < 136$ GeV/c^2 dijet mass window was 87% efficient for the CDF analysis while this analysis found roughly 90%. This small difference in signal shape accounts for a 3% change in efficiency. Finally, the inclusion of the ZH cross-efficiency adds 6% to the signal expectation. Table 12 shows the percent increase in the value of $S/\sqrt{B}$ for each step along with the corresponding $S/\sqrt{B}$ with this increase included. With these factors, we find that the CDF and DØ WH analyses agree to within 2% in the value of $S/\sqrt{B}$. At this point, before the inclusion of the neural network, we have shown that we are able to reproduce the CDF $WH \to \ell\nu b\bar{b}$ analysis sensitivity.

4.2 Addition of Neural Network Techniques

After confirming the baseline normalization and event expectation for the WH analysis, we now move to evaluating the increase in sensitivity obtained by employing neural network techniques. The $t\bar{t}$ NN used in the ZH analysis included purely hadronic input variables and can be easily modified to select the WH signal. The only variable of the $t\bar{t}$ NN that

must be modified is the net p_T imbalance of the $\not\!\!E_{\rm T} + b\bar{b}$ system. This variable was designed to exploit the hypothesis that the $Z \to \nu\bar{\nu} + H \to b\bar{b}$ system has zero net p_T. We can adapt this variable to the WH system by calculating instead the net p_T imbalance of the ℓ + $\not\!\!E_{\rm T}$ + $b\bar{b}$ system. This variable can be seen in Figure 14 and the result is very similar to the corresponding variable derived for the $ZH \to \nu\nu b\bar{b}$ analysis. The remaining input variables to the WH $t\bar{t}$ NN are identical to those used in the ZH $t\bar{t}$ NN (see Section 3). An $8 \times 16 \times 1$ NN was generated and trained using $WH \to e, \mu\nu b\bar{b}$ signal and $t\bar{t} \to \ell\nu jj$ background Monte Carlo events. The training was performed using events with one good electron or muon, with $\not\!\!E_{\rm T} > 20\,{\rm GeV}$, and which pass the Z veto. The output of the WH $t\bar{t}$ NN can be seen in Figure 15 for WH signal and $t\bar{t} \to \ell\nu jj$ background.

After obtaining the NN distribution, the cut value was determined by maximizing the value of $S/\sqrt{B}$ for the full signal and background sample. For the $m_H = 115$ GeV/c^2 mass point, the maximum value was found to be $NN > 0.90$. The analysis was then evaluated after adding this additional selection criterion and the corresponding NN efficiencies are shown for signal and background in Tables 13-15. The increase in sensitivity can then be calculated directly using the selection efficiencies with and without the NN selection cut. Table 16 shows the expected number of signal and background events with and without the NN. Also listed in Table 16 are the change in $S/\sqrt{B}$ and the corresponding luminosity factor this would result in (normalized to the DØ WH analysis without a NN selection cut applied). Here we find a luminosity factor of 1.75 when including both the WH signal and the ZH signal cross-efficiency. This number rises slightly when evaluated using WH signal alone, as the ZH signal has a lower efficiency for the NN selection. We can compare this number with the NN factor of 1.6 obtained in the CDF Run I analysis to account for the expected increase in sensitivity gained by adding a NN analysis step.

We conclude that the NN factor used for the combined result was both appropriate and conservative. Furthermore, it should be noted that the luminosity factor of 1.75 found in this study is itself conservative as no effort was made to optimize the WH analysis or the NN. A full optimization would incorporate more information about the selected lepton into the analysis and could gain additional discrimination between signal and background in this way.

	Signal	Bkgd	$\Delta S/\sqrt{B}$	$S/\sqrt{B}$
Baseline result	-	-	-	0.45
Lepton ID Factor	1.08	1.08	+4%	0.47
b-Tagging Factor	1.14	1.14	+7%	0.50
Mass Window Factor	1.03	1.00	+3%	0.52
ZH Cross-Efficiency	1.06	1.00	+6%	0.55

Table 12: Values of increased signal and background efficiency between the CDF WH analysis and the DØ WH analysis (prior to a NN selection cut). Each factor is used to calculate an increase in $S/\sqrt{B}$. These factors are then sequentially applied to the baseline CDF result for a final value of $S/\sqrt{B} = 0.55$.

Process	$WH \to e\nu b\bar{b}$	$WH \to \mu\nu b\bar{b}$	$WH \to \tau\nu b\bar{b}$
Cross Section (pb)	0.186	0.186	0.186
Branching Ratio	0.732×0.107	0.732×0.107	0.732×0.107
1 e, μ	65.7	55.6	11.3
$\not\!\!E_{\rm T} > 20\,{\rm GeV}$	85.4	89.3	89.2
Pass Z Veto	99.9	98.6	99.7
Jet Selection	74.3	76.6	71.1
Kinematic Selection	84.2	82.7	81.0
2 b-Tagged Jets	31.9	32.7	31.1
Mass Window	89.6	89.1	88.2
NN Cut	95.0	95.9	82.7
Acceptance (w/o NN)	10.0	9.04	1.58
Acceptance (w/ NN)	9.50	8.67	1.31
Trigger Efficiency	95.0	95.0	95.0
Events in 1 fb^{-1}(w/o NN)	1.38	1.25	0.22
Events in 1 fb^{-1}(w/ NN)	1.31	1.19	0.18

Table 13: Selection efficiencies (%) for $WH \to \ell\nu b\bar{b}$ signal Monte Carlo with m_H =115 GeV/c^2. The expected number of events is evaluated both with and without the NN selection cut. A 10% dijet mass resolution is assumed. The branching ratio is the product of BR($H \to b\bar{b}$) multiplied by BR($W \to e\bar{\nu}$), similarly for μ and τ decays of the W boson.

Process	$ZH \to ee b\bar{b}$	$ZH \to \mu\mu b\bar{b}$	$ZH \to \tau\tau b\bar{b}$
Cross Section (pb)	0.108	0.108	0.108
Branching Ratio	0.732×0.034	0.732×0.034	0.732×0.034
1 e, μ	88.9	80.6	21.9
$\not\!\!E_{\rm T} > 20\,{\rm GeV}$	32.0	53.2	76.3
Pass Z Veto	45.6	59.9	99.6
Jet Selection	74.3	77.5	48.7
Kinematic Selection	62.5	67.7	59.5
2 b-Tagged Jets	27.1	31.4	28.0
Mass Window	88.0	87.2	88.0
NN Cut	78.1	81.0	69.8
Acceptance (w/o NN)	1.44	3.69	1.19
Acceptance (w/ NN)	1.12	2.99	0.83
Trigger Efficiency	95.0	95.0	95.0
Events in 1 fb^{-1}(w/o NN)	0.04	0.09	0.03
Events in 1 fb^{-1}(w/ NN)	0.03	0.08	0.02

Table 14: Selection efficiencies (%) for $ZH \to \ell\ell b\bar{b}$ signal Monte Carlo with m_H =115 GeV/c^2. The expected number of events is evaluated both with and without the NN selection cut. A 10% dijet mass resolution is assumed. The branching ratio is the product of BR($H \to b\bar{b}$) multiplied by BR($Z \to$e$^+$e$^-$), similarly for μ and τ decays of the Z boson.

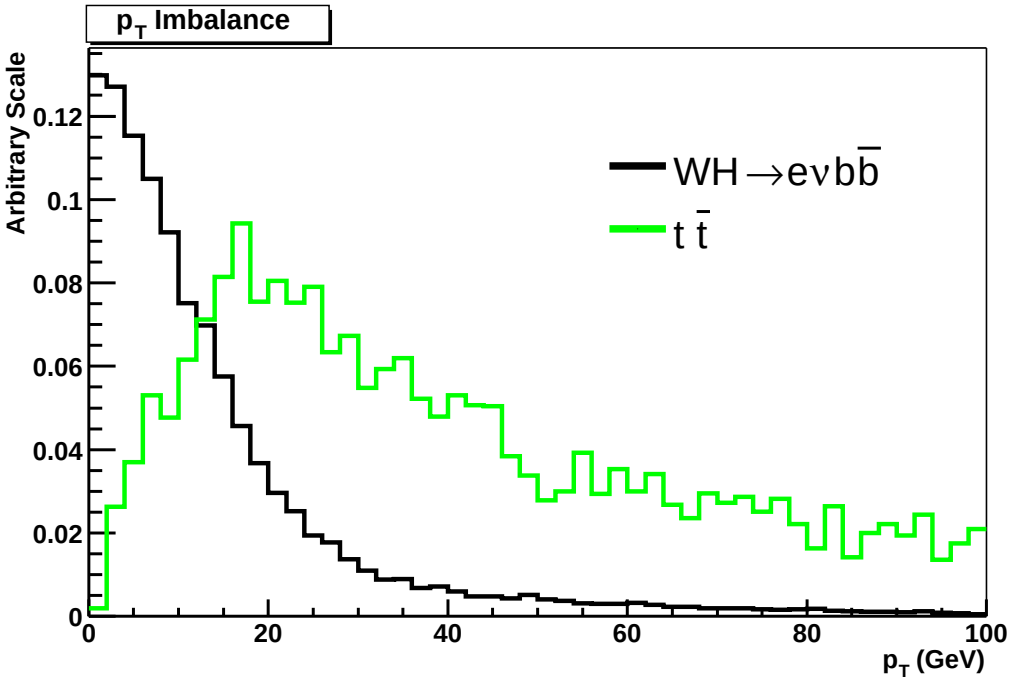

Figure 14: Net p_T imbalance input to the WH $t\bar{t}$ NN.

Background Source	$Wb\bar{b}$	$t\bar{t}(\ell\nu jj/\ell\nu\ell\nu)$	$t(W^*)$	$t(Wg)$	WZ	ZZ
Cross Section (pb)	10.6	7.0	0.80	2.24	3.2	1.7
Branching Ratio	0.32	0.44/0.10	0.32	0.32	1.00	1.00
1 e, μ	41.8	42.8/49.4	40.3	42.7	18.2	13.5
$\not\!\!E_{\rm T} > 20\,{\rm GeV}$	91.8	91.3/93.4	91.6	89.5	79.1	52.0
Pass Z Veto	99.6	99.3/89.8	99.9	99.6	91.5	67.2
Jet Selection	48.0	38.8/76.4	71.0	54.7	52.8	48.4
Kinematic Selection	65.9	32.3/40.6	80.4	84.1	80.7	62.0
2 b-Tagged Jets	18.0	15.1/35.5	30.0	2.66	5.63	6.18
Mass Window	14.5	25.3/24.6	26.1	23.2	12.7	39.3
NN Cut	57.6	16.9/50.2	60.1	58.1	84.5	67.3
Acceptance (w/o NN)	0.31	0.19/1.12	1.65	0.11	0.04	0.03
Acceptance (w/ NN)	0.18	0.03/0.56	1.00	0.06	0.03	0.02
Trigger Efficiency	95.0	95.0	95.0	95.0	95.0	95.0
Events in 1 fb^{-1}(w/o NN)	10.1	5.36/7.59	4.15	0.77	1.22	0.55
Events in 1 fb^{-1}(w/ NN)	5.78	0.90/3.82	2.49	0.44	1.03	0.37

Table 15: Selection efficiencies (%) for WH background Monte Carlo. The expected number of events is evaluated both with and without the NN selection cut. The branching ratio is BR($W \to \ell\bar{\nu}$) and includes combinatorical factors.

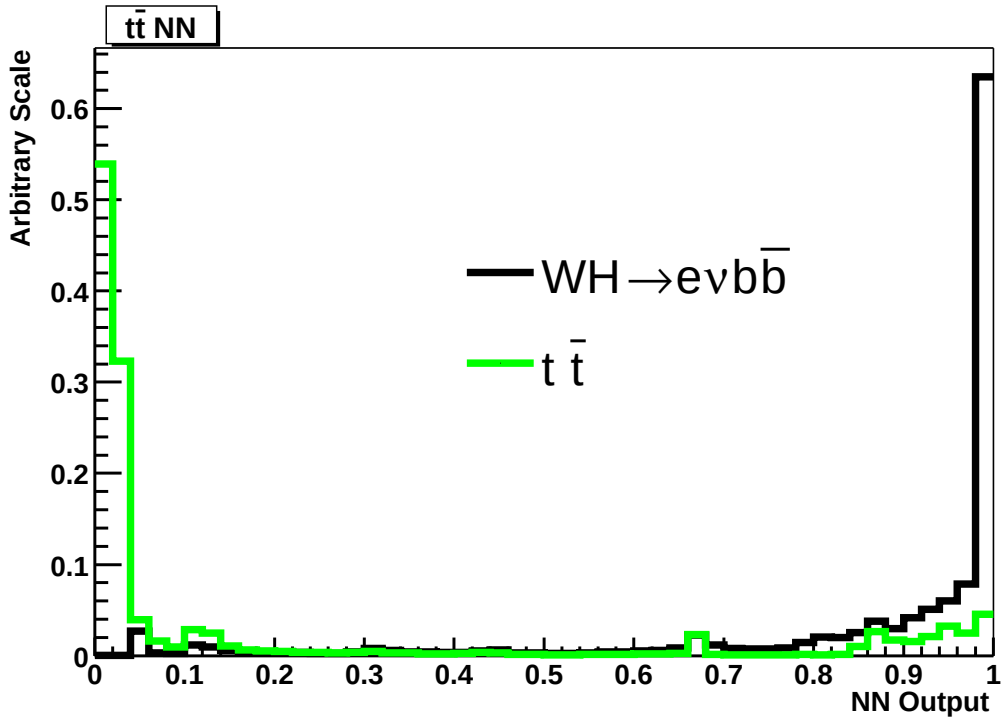

Figure 15: WH $t\bar{t}$ NN output.

Method	No NN	NN Applied
Events (1 fb^{-1})		
WH	2.84	2.68
ZH	0.16	0.12
Signal	3.00	2.80
$t\bar{t}$	13.0	4.72
$Wb\bar{b}$	10.1	5.78
$t(W^*)$	4.15	2.49
$t(Wg)$	0.77	0.44
WZ	1.22	1.03
ZZ	0.55	0.37
Background	29.1	14.5
$S/\sqrt{B}$	0.55	0.73
Lumi Factor	(1.00)	1.75

Table 16: Results for the WH search. Expected number of signal and background events in 1 fb^{-1} in a 100–136 GeV/c^2 mass window, assuming 10% $b\bar{b}$ mass resolution. The expected number of events is evaluated with and without the application of a NN selection. The increase in sensitivity due to the NN and the corresponding luminosity factor are shown as well. The luminosity factor is normalized to the DØ WH analysis with no NN cut applied.

5 Studies of Dijet Invariant Mass Resolution

To extract the Higgs boson signal from the large physics backgrounds it is necessary to rely on the invariant mass of the $b\bar{b}$ system, $m_{b\bar{b}}$. Once the appropriate corrections have been applied to the b jets, the Higgs boson signal will peak at m_H, while the backgrounds from $W+$jets, $t\bar{t}$, and single top production have smooth distributions in $m_{b\bar{b}}$. The background from WZ production followed by $Z \to b\bar{b}$ produces a peak in the $m_{b\bar{b}}$ distribution, but centered at $m_Z = 91\,\mathrm{GeV}/c^2$, which is at least $20\,\mathrm{GeV}/c^2$ less than the values of m_H considered in this study. Attaining the best possible $b\bar{b}$ mass resolution is crucial for establishing a signal with least amount of integrated luminosity.

In the SHWG study, the projections were based on counting events in a mass window in $m_{b\bar{b}}$. This procedure requires absolute normalization of the backgrounds (and an estimate of the associated systematic error). For the SHWG study, it was assumed a resolution of $\sigma(m_{b\bar{b}})/m_{b\bar{b}} = 10\%$ could be achieved, although at that time, no studies showed explicitly this resolution was possible. A 20% increase in mass resolution to $\sigma(m_{b\bar{b}}) = 12\%$ was found to increase the required integrated luminosity to achieve the same sensitivity by 20%. The ultimate resolution was reported to be $\sigma(m_{b\bar{b}}) = 8\%$, which is due to effects from jet fragmentation, soft gluon radiation, and neutrinos.

In this study we have performed a fit to the $m_{b\bar{b}}$ distribution. For a particular value of m_H, the observed rate of events outside the signal mass window (*i.e.*, the sidebands) provides a constraint on the normalization of the combination of backgrounds. This approach requires understanding the shape of the $m_{b\bar{b}}$ distributions of the backgrounds and the effect of the jet corrections on these shapes. For our study, we have assumed that the mass resolution follows a Gaussian distribution, and we have examined mass resolutions in the range $10\% < \sigma(m_{b\bar{b}}) < 20\%$. We find fitting the mass distribution instead of simply counting events in a mass window corresponds to about a 20% increase in effective luminosity, assuming no systematics uncertainties on the background estimations. The effects due to uncertainties in the predictions of the mass distributions of the backgrounds and non-Gaussian tails in the resolution function of $m_{b\bar{b}}$ for the signal are discussed in Section 8.3.

5.1 Jet Energy Resolution of the DØ Detector

The dijet mass resolution is directly related to the energy resolution of the jets. For a jet of $E_T = 55$ GeV, corresponding to a typical jet E_T of the b jets coming from the decay of the Higgs boson with $m_H \sim 100$ GeV/c^2, the fractional jet E_T resolution used in the SHWG simulation was $\sigma(E_T)/E_T \sim 13.5\%$. This jet E_T resolution results in a $H \to b\bar{b}$ mass resolution of ∼15% for Higgs boson masses ~ 100 GeV/c^2 for events with only two jets. In the final combination of all channels and interpretation of the results, however, a 30% improvement on the mass resolution was assumed, *i.e.*, a 10% mass resolution at $m_H \sim 100$ GeV/c^2. The 30% improvement on the SHWG jet E_T resolution at $E_T = 55$ GeV would correspond to $\sigma(E_T)/E_T \sim 9.5\%$. The jet E_T resolution of the DØ calorimeter measured from Run I data at $E_T = 55$ GeV and in the central pseudorapidity region was 11.0%. The Run II DØ resolution at the same E_T and η is 13.9% (for both 0.5 and 0.7 cones). The comparison of the various resolutions is summarized in Table 17. In order to achieve the 10% dijet mass resolution, we need to improve the current resolution by ∼30%. There

	$\sigma(E_T)/E_T$ (%)
SHWG	13.5
30% improvement on SHWG	9.5
DØ Run I data, $R_{cone} = 0.7$	11.0
DØ Run II data, $R_{cone} = 0.7$	13.9
DØ Run II data, $R_{cone} = 0.5$	13.9

Table 17: Jet E_T resolution for jets of $E_T = 55$ GeV in the central pseudorapidity region. The Run II jets have been reconstructed with version p13.05 of the DØ software, and their E_T's have been corrected with the JetCorr v4.1 jet energy scale correction.

are several sources for improvement: improved calorimeter calibration, use of additional detector subsystems (*e.g.*, tracking chambers), and advanced algorithms that use full event information. Some of these approaches are discussed below.

5.2 Jet Correction Algorithms

The CDF study examined a series of jet energy corrections to obtain the best current understanding of the jet energy resolution and therefore dijet mass resolution. To understand the resolution of the invariant mass of a two-jet system, it is crucial to use data, since Monte Carlo simulation may not reproduce all of the important details due to physics and detector effects. We have a good understanding of jets produced in association with photons (which are measured well in the calorimeter) and $Z \to \ell^+\ell^-$ decays. In particular, we can use this associated production to understand and develop jet corrections for these "generic" jets. These jets are dominated by gluons and light quarks. Higgs boson decays are special since they involve b quarks. The fragmentation of b quarks is harder than the fragmentation of gluons and light quarks, and B hadrons have a large ($\sim 40\%$) semileptonic branching fraction. These semileptonic decays produce high p_T muons and neutrinos that produce little energy (minimum ionizing from μ), or no energy (in the case of neutrinos), in the calorimeter, resulting in an underestimate of the jet energy if only calorimetric information is used.

We developed a series of corrections to the observed raw jet energy. The impact of these corrections is shown in Figure 16. The four figures correspond to the dijet mass at four different stages of the correction:

1. **Raw jet energies** (upper left): These are simply the jets from a calorimeter-energy clustering algorithm using a cone of $R = 0.4$. The initial core resolution is 18%.

2. **Calorimeter/Tracking Correction** (upper right): The corrections use information from the calorimeter towers and from reconstructed tracks (in the central region only, however, precise tracking is not required, so these corrections should be possible in the endcap calorimetry as well). These corrections are derived from data (*e.g.*, by using transverse momentum balancing in dijet events) and Monte Carlo. The core resolution improves to 12%.

3. **b-quark Specific** (lower left): These corrections are determined from Monte Carlo and are specific for b-quark jets. The corrections depend on whether a low p_T muon or electron is observed in the jet. After this correction the core resolution is 11%.

4. **Advanced Algorithm** (lower right): The previous three corrections have been studied and used by CDF for several years. For this study of the sensitivity to a Higgs boson signal, an additional technique was developed. This approach creates jet corrections which depend on the topology of the event (*e.g.*, how close is another jet to the jet that is being corrected). This final correction shows promise of actually achieving a dijet mass resolution of 10%.

Figure 16 shows the dijet mass distribution when both jets are in the central calorimeter. The predicted changes in resolution when one or both jets are in the endcap (plug) calorimeter are shown in Figure 17. The change in resolution when one or both jets falls into the endcap has not been included in the present study, however, it should be straightforward to include them in future work.

The crucial issue is whether the dijet energy resolutions predicted with Monte Carlo simulation can be achieved in data. In Run I the inclusive muon trigger ($p_T(\mu) > 8\,\mathrm{GeV}/c$) was used to collect a sample of $Z \to b\bar{b}$ decays[14]. The extracted signal is shown in Figure 18. Corrections applied to the data to improve the mass resolution were tracked by the Monte Carlo. Although this comparison was limited by the small statistics of the signal in the data, the results were very encouraging.

In Run II we are using the Silicon Vertex Tracker (SVT) to trigger on $Z \to b\bar{b}$. It is expected that with $300 - 400\,\mathrm{pb}^{-1}$ of data we should be able to extract a significant signal and begin to study jet energy corrections for $m_{b\bar{b}}$ with adequate statistics. As we do not have this signal yet, for this study we are assuming we can achieve a Gaussian resolution of $\sigma(m_{b\bar{b}})/m_H = 10\%$.

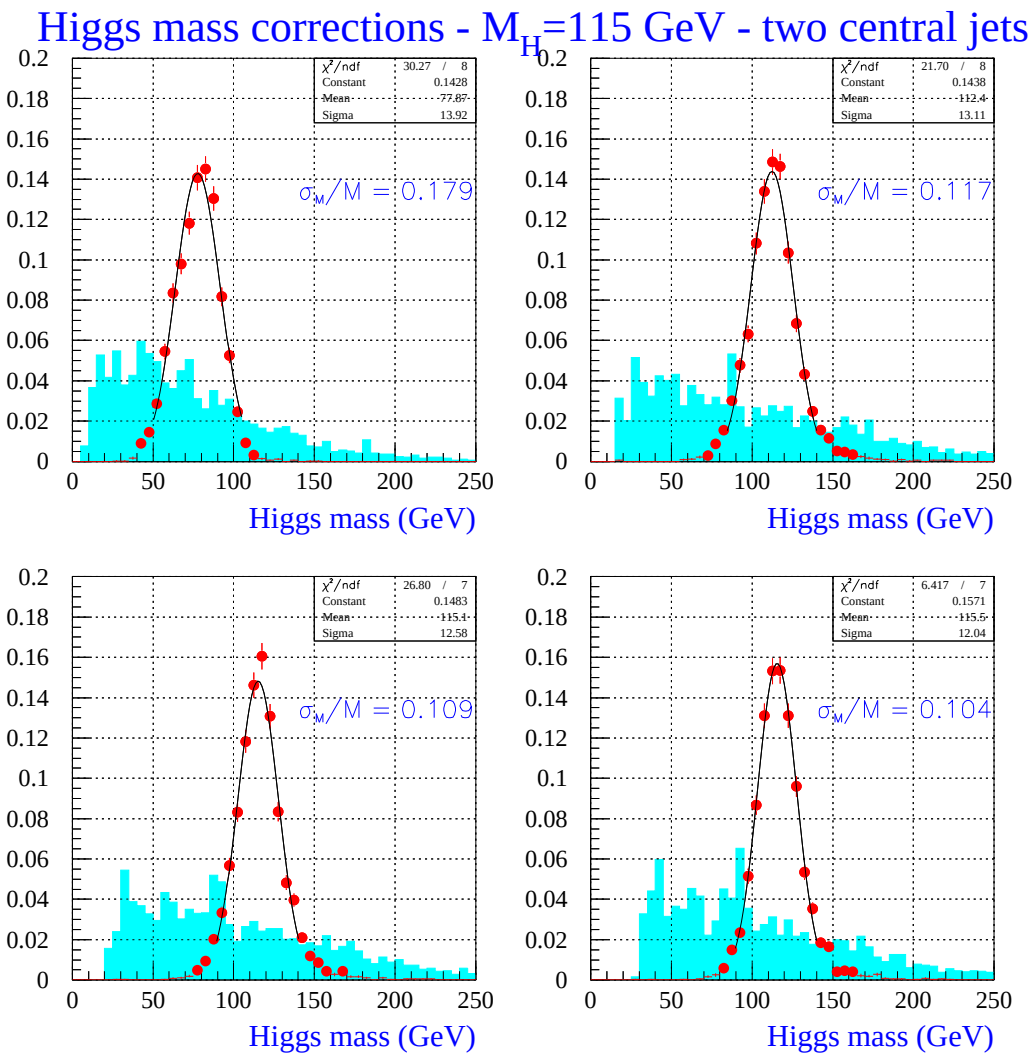

Figure 16: The distribution of $m_{b\bar{b}}$ for the Higgs boson signal (points) for $m_H = 115\,\mathrm{GeV}/c^2$ and the expected combination of backgrounds (histogram). The distributions have been normalized to the same area. The core of the distribution for the Higgs boson signal has been fit with a single Gaussian and the resolution divided by m_H is reported. These distributions are for the case where both jets are in the central calorimeter; the four distributions correspond to four sets of jet corrections, which are summarized in the text.

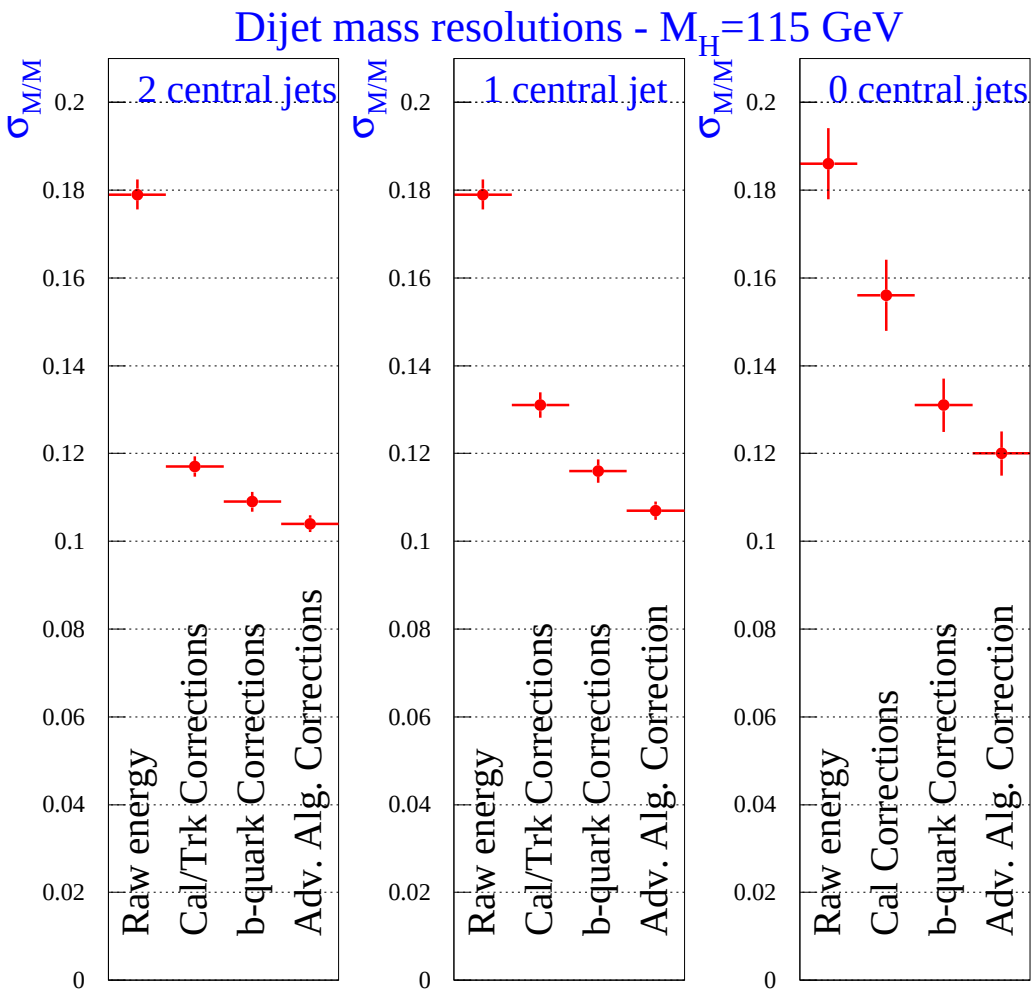

Figure 17: The width of the central core of the $m_{b\bar{b}}$ distribution for the four different sets of jet corrections outlined in the text when both jets are in the central calorimeter (left), one jet is central and the other is in the endcap calorimeter (center), and both jets are in the endcap (right). For jets in the endcap calorimeter no tracking correction is applied. However, with the development of forward tracking algorithms this should be possible in the future.

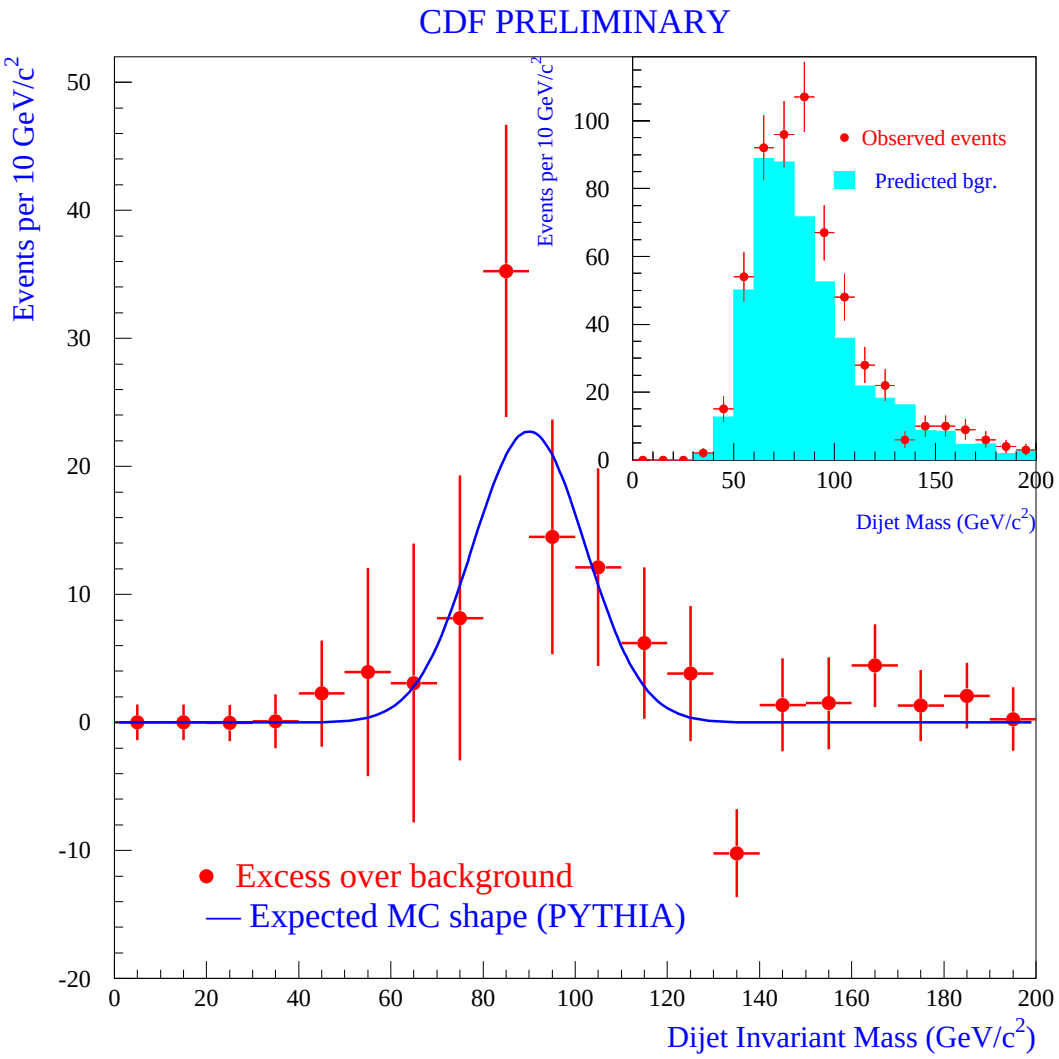

Figure 18: The $Z \to b\bar{b}$ signal extracted from a Run I data sample collected with an inclusive muon trigger requiring $p_T(\mu) > 8\,\mathrm{GeV}/c$. The curve shows the expected distribution predicted by Monte Carlo. The agreement between data and Monte Carlo is good and the comparison is limited by the statistics of the data.

6 Sensitivity Estimation

In order to quantify the Higgs search sensitivity, we calculate the integrated luminosity required for a given experimental outcome. We consider three levels of possible experimental observations: (1) excluding standard model Higgs boson production at the 95% confidence level (CL); (2) observing an excess number of events at the 3σ level; (3) observing an excess number of events at the 5σ level. We used two techniques to calculate these thresholds as a function of Higgs mass. The first is based on a Bayesian approach and is very similar to the method used in the SHWG study. The second is an approach used at LEP called the Confidence Level for Signal (CL_s) method [15].

The two techniques rely on performing pseudoexperiments with a mean event yield and a fixed amount of luminosity. At a given luminosity, we calculate the fraction of pseudoexperiments that exceed the three levels of observations listed above. For the case of the 95% CL exclusion, the pseudoexperiments have no signal contribution. The procedure then makes a scan through integrated luminosities.

6.1 Bayesian Approach

Figure 19 shows the result of many pseudoexperiments using the Bayesian approach. The top plot uses pseudoexperiments that do not include signal events and are used to establish 95% CL on the cross section. The y-axis is normalized so that a value of 1 corresponds to the standard model cross section for $m_H = 115$ GeV/c^2. The x-axis is integrated luminosity per experiment. At any given integrated luminosity, there is a range of limits on the cross section that can be set. The bottom plot shows pseudoexperiments that have signal included and are used to measure the significance of the excess of events over background. The x-axis once again is integrated luminosity. This plot shows that at low integrated luminosity that the chance of having an experiment that observes more than 3σ excess is rare.

Using the scatter plots from Figure 19, we can determine the fraction of pseudoexperiments that satisfy (fall above) a particular criteria. Figure 20 shows the fraction of experiments that satisfy our three threshold criteria as a function of integrated luminosity. In the SUSY-Higgs Working Group report, the luminosity threshold was set at the 50% point. It is clear from these distributions that our *one* trial (Run II) has a wide-range of possible outcomes requiring substantially less or substantially more integrated luminosity, relative to the median expectation.

6.2 Confidence Level for Signal Method

The predicted shapes of the signal distributions in the final sample of selected events enhances the sensitivity of the search. The method applied here assumes that there is a background shape for the reconstructed $b\bar{b}$ mass from a set of known background processes, or data-derived background processes. The next step is to compare the superposition of the predicted signal distribution on top of the background for every mass bin in the analysis. This comparison is done with Poisson counting statistics. A likelihood ratio is formed by dividing the "signal + background" ($S + B$) Poisson likelihood by the "background only"

(B) likelihood, as follows:

$$Q = \frac{\mathcal{L}_{S+B}}{\mathcal{L}_B} = \frac{\Pi_i^N e^{-(S_i+B_i)}(S_i+B_i)^{n_i}}{\Pi_i^N e^{-B_i} B_i^{n_i}} \quad . \tag{3}$$

The resulting quantity, Q, is the instantaneous ratio of the probabilities for the two hypotheses for a given set of observations, n_i, with $Q = 1$ being the dividing line between which is the more likely hypothesis to describe the data. The negative logarithm of the ratio has a compact form:

$$-\ln Q = S - \sum_i n_i \ln\left(1 + \frac{S_i}{B_i}\right) \tag{4}$$

where $S = \sum_i S_i$. The distance between the medians of the two hypotheses in units of $\ln Q$ is an estimate of the variance between the two hypotheses:

$$\Delta \ln Q = -\ln \frac{Q_{S+B}}{Q_B} = \sum_i S_i \ln\left(1 + \frac{S_i}{B_i}\right) \quad . \tag{5}$$

For large backgrounds the single bin estimator is $\sqrt{\Delta \ln Q} \approx S/\sqrt{B}$, which agrees with the SHWG method.

The log likelihood ratio estimator is linear with luminosity and is additive in the number of channels and the number of bins in the mass distributions. For the $\nu\bar{\nu}b\bar{b}$ analysis for a mass window of 100–136 GeV/c^2 and $m_H = 115$ GeV/c^2, the number of expected signal and background events are $S = 3.80$ and $B = 19.6$, respectively, for 1 fb^{-1} of integrated luminosity per experiment. The single bin estimator gives $S/\sqrt{B} = 0.86$ or, using the log likelihood ratio estimator, $\Delta \ln Q = 0.67$. Breaking the analysis into 2 GeV/c^2 bins gives the signals and backgrounds shown in Table 18. The ratio S/B is found to vary by a factor of 2-3 over this range.

Mass Bin (GeV/c^2)	101	103	105	107	109	111	113	115	117
Signal	0.11	0.14	0.17	0.20	0.23	0.26	0.29	0.30	0.29
Background	1.97	1.80	1.62	1.41	1.24	1.13	1.07	1.02	0.98
S/B	0.07	0.09	0.12	0.17	0.22	0.27	0.31	0.33	0.33

Mass Bin (GeV/c^2)	119	121	123	125	127	129	131	133	135
Signal	0.28	0.25	0.22	0.19	0.14	0.10	0.07	0.05	0.04
Background	0.94	0.90	0.87	0.83	0.79	0.75	0.72	0.69	0.65
S/B	0.32	0.30	0.28	0.24	0.20	0.14	0.10	0.09	0.07

Table 18: Signal and background values for 2 GeV/c^2 mass bins in the $\nu\bar{\nu}b\bar{b}$ analysis with $m_H = 115$ GeV/c^2.

The sensitivity using these bins of the mass distribution is

$$\Delta \ln Q_{\nu\bar{\nu}b\bar{b}} = \sum_i S_i \ln(1 + S_i/B_i) = 0.81 \tag{6}$$

corresponding to a 21% increase in equivalent luminosity due to the shape information. The full set of mass distributions for the $\nu\bar{\nu}b\bar{b}$ is plotted in Figure 21 corresponding to 10 fb^{-1} for a single experiment.

A similar analysis is performed on the $\ell\bar{\nu}b\bar{b}$ channel. For the mass window of 100–136 GeV/c^2 and $m_H = 115$ GeV/c^2, the number of expected signal and background events are $s = 2.50$ and $b = 30.3$, respectively, for 1 fb^{-1} of integrated luminosity per experiment. The single bin estimator gives $S/\sqrt{B} = 0.45$ or $\Delta \ln Q = 0.20$. With the neural network efficiencies in Table 20 applied, as described in Section 7, the number of expected signal and background events are $s = 2.36$ and $b = 16.8$, respectively, for 1 fb^{-1} of integrated luminosity, and the single bin estimator gives $S/\sqrt{B} = 0.58$ or $\Delta \ln Q = 0.31$. The ratio of $\Delta \ln Q$ with and without the neural network efficiencies gives an improvement factor of 1.6 in effective luminosity. Breaking the analysis with neural network efficiencies applied into 2 GeV/c^2 bins gives the following table (Table 19) of signals and backgrounds. The ratio S/B is fairly flat, but varies by a factor of three on the edge bins compared to the central region.

Mass Bin (GeV/c^2)	101	103	105	107	109	111	113	115	117
Signal	0.09	0.11	0.13	0.15	0.17	0.18	0.18	0.18	0.17
Background	1.46	1.37	1.26	1.16	1.09	1.03	0.98	0.94	0.90
S/B	0.06	0.08	0.11	0.13	0.15	0.17	0.19	0.20	0.20

Mass Bin (GeV/c^2)	119	121	123	125	127	129	131	133	135
Signal	0.17	0.16	0.15	0.13	0.11	0.09	0.07	0.06	0.04
Background	0.86	0.83	0.81	0.78	0.76	0.74	0.72	0.70	0.69
S/B	0.20	0.19	0.18	0.16	0.14	0.12	0.10	0.08	0.06

Table 19: Signal and background values for 2 GeV/c^2 mass bins in the $\ell\bar{\nu}b\bar{b}$ analysis with $m_H = 115$ GeV/c^2.

The sensitivity using these bins of the mass distribution is

$$\Delta \ln Q_{\ell\bar{\nu}b\bar{b}} = \sum_i S_i \ln(1 + S_i/B_i) = 0.34 \tag{7}$$

corresponding to a 10% increase in equivalent luminosity due to the shape information. The improvement from the use of the mass distribution is much less than observed in the $\nu\bar{\nu}b\bar{b}$ analysis. This comes from the slower variation in S/B within these bins of the mass distribution with more high mass background. The full set of mass distributions for the $\ell\bar{\nu}b\bar{b}$ analysis is plotted in Figure 22 corresponding to 10 fb^{-1} for a single experiment.

7 Combining Results: WH and ZH Modes

We combine the WH and ZH channels for the two experiments using the dijet mass shapes and normalizations from the two studies. Each channel is multiplied by two in order to

account for the two experiments. In addition, we include scale factors for the following effects.

1. **Inclusion of $ZH \to \ell\ell bb$ Channel:** This channel was not reanalyzed. To include the additional sensitivity from this channel, we scale *both* the signal and background in the ZH $\to \nu\nu bb$ channel by 1.33. This factor is based on the previous ratio of single-bin sensitivities from the SHWG report.

2. **Impact of Neural Network on WH Channel:** An estimate of the improvement to a cuts-based analysis using a neural net (NN) application to this channel was studied in a CDF Run I analysis. This predicted an overall factor of 1.6 in effective luminosity. The detailed study in this report described in Section 4 estimates the neural network efficiencies for signal and for each background. These efficiencies, listed in Table 20, are applied to the CDF baseline analysis with a 7% increase to the backgrounds to match the 1.6 effective luminosity factor from the previous study.

3. **Overlap of the ZH and WH Channels:** The events selected by the ZH and WH analyses by a single experiment are chosen to have zero overlap by construction. It was verified in Section 4 that the CDF WH event selection was reproducible by the DØ WH analysis and that this selection was tighter in terms of the lepton finding efficiency than the corresponding lepton veto used in the ZH analysis from DØ. Therefore, the effect of an event sample overlap between CDF WH and DØ ZH analyses is assumed to have a negligible effect on the sensitivity. In this study, the ZH and WH analyses are treated as orthogonal with no overlap between them.

Table 20 gives a summary of the number of events selected by the $\ell\bar{\nu}b\bar{b}$ and $\nu\bar{\nu}b\bar{b}$ analyses for a 100–136 GeV/c^2 mass window and a Higgs boson mass of $m_H = 115$ GeV/c^2. The two statistical techniques used to extract luminosity thresholds report slightly different requirements for the integrated luminosity. The computed integrated luminosity thresholds are listed in Table 21. To set the scale, for 3 fb^{-1} of integrated luminosity per experiment, this predicts 37 selected Higgs events summed over the two analyses and the two experiments within the mass window for $m_H = 115$ GeV/c^2, not including the additional events from the $\ell\ell b\bar{b}$ analysis.

Figure 23 shows the 95% CL limit using the CL$_s$ method as a function of integrated luminosity when the WH and ZH channels are combined. The three plots show Higgs masses of 115, 120, and 130 GeV/c^2. For the 95% CL limit on the cross section, there is little difference between the Bayesian approach and the CL$_s$ approach. The dashed line shows where 50% of the pseudoexperiments lie above and below for each integrated luminosity. The green (inner) envelope contains 68% of the pseudoexperiments and the yellow (outer) envelope contains 95% of the pseudoexperiments. With 10 fb^{-1} we have ∼85% chance to exclude a standard model Higgs up to a mass of 130 GeV/c^2 and on average we would only need ∼4 fb^{-1} to do so.

The results presented are an analysis of the statistical power of the data assuming we have perfect understanding of the background rates and the shape of the $m_{b\bar{b}}$ distributions of both the signal and the backgrounds. Systematic effects such as non-Gaussian tails in the $m_{b\bar{b}}$ resolution and errors in the shapes of the $m_{b\bar{b}}$ distributions of the backgrounds will

Search channel	$\nu\bar{\nu}b\bar{b}$ (w/NN)	$\ell\bar{\nu}b\bar{b}$	$\ell\bar{\nu}b\bar{b}$ (w/NN)	NN eff.(%)
WH signal	1.5	2.5	2.4	94.4
ZH signal	2.3	–	–	–
Number of Signal Events	3.8	2.5	2.4	–
$t\bar{t}$	2.2	10.0	3.9	39.0
$t(W^*)$	0.7	3.5	2.2	64.3
$t(Wg)$	0.5	1.1	0.7	61.8
$Wb\bar{b}/Zb\bar{b}$	3.3	14.7	9.1	61.6
WZ/ZZ	2.7	1.0	0.9	90.0
QCD	10.2	–	–	–
Number of Background Events	19.6	30.3	16.8	–

Table 20: The number of events selected per experiment by the $\nu\bar{\nu}b\bar{b}$ and $\ell\bar{\nu}b\bar{b}$ analyses for 1 fb^{-1}, a 100–136 GeV/c^2 mass window and a Higgs boson mass of $m_H = 115$ GeV/c^2. The second column is the baseline CDF $\ell\bar{\nu}b\bar{b}$ analysis. The third column corresponds to the expected number of events from the $\ell\bar{\nu}b\bar{b}$ analysis with the neural network efficiencies from Section 4 applied. These efficiencies are listed in the fourth column with the backgrounds scaled up by 7% to correspond to an overall 1.6 effective luminosity factor.

add to this challenge. As discussed in Section 8, controlling these systematic effects will be crucial to this analysis. In the future, we will have to rely on our data to understand the backgrounds and determine the dijet mass resolution.

Figure 24 summarizes the required luminosity thresholds in the same format as the plot that is commonly used to summarize the findings of SUSY-Higgs Working Group. The thresholds are defined by the luminosity required to have 50% of the pseudoexperiments satisfy the criteria. The results of the SHWG are superimposed on these plots. The lower edge of the SHWG bands include the effect of some systematics. The 30% width of the SHWG band is a safety factor included to account for degradations in sensitivity that were not included in the study. The results of the present study lie below the results of the SHWG report. The present study gives the projected statistical power of the data only: no systematics are included. The effect of systematics will cause these bands to move up and could be very significant. A list of systematic errors appears in Section 8. The impact of background and signal normalization is discussed. The width of the bands from this study is approximately 10% and is due to the difference between the results from the CL$_s$ method (lower edge) and the results of the Bayesian method (upper band).

8 Systematic Errors

The results of the SHWG shown in Figure 1 include an estimate of the effect of systematic uncertainties on the backgrounds. The uncertainty on the background rate was determined in the following way: if the product of the integrated luminosity $\mathcal{L}$ and the background cross section σ_B was less than 100 events, a 10% uncertainty was assigned to the background

m_H (GeV/c^2)	110	115	120	130
95% CL: CL_s	1.17	1.35	1.70	3.96
95% CL: Bayesian	1.23	1.43	1.78	4.24
95% CL: SHWG	1.30	—	2.20	4.15
3σ: CL_s	2.57	2.97	3.74	8.72
3σ: Bayesian	2.83	3.31	4.14	9.80
3σ: SHWG	3.53	—	5.69	9.67
5σ: CL_s	6.79	7.87	9.90	23.07
5σ: Bayesian	7.63	9.00	11.22	26.59
5σ: SHWG	11.07	—	16.4	28.6

Table 21: The calculated luminosity thresholds in fb^{-1} from the combination of two experiments and the WH and ZH channels. All scale factors described above are included: the signal and background are multiplied by a factor of 1.33 in the ZH channel to account for $\ell\ell b\bar{b}$. The WH channel has the neural network efficiencies applied. These efficiencies are listed in Table 20. The Bayesian and CL_s methods report slightly different luminosity thresholds. The CL_s and Bayesian numbers are a statement about the statistical power of the data and include no systematic errors. The numbers for the SHWG correspond to the lower edge (most optimistic) of the bands in their summary plot (Figure 24).

normalization; when $B = \mathcal{L} \cdot \sigma_B > 100$, the systematic uncertainty on the background was $100\%/\sqrt{B}$. This anticipated an improvement in the understanding of the backgrounds as more data was accumulated. The lower edge of the bands shown in Figure 1 include these systematic effects. The study reported that without these systematic errors on the background rates, the integrated luminosity thresholds would be approximately 30% to 50% lower [2].

Due to the limited time for this study, we have not evaluated the effect of systematic uncertainties. In this section we discuss the major sources of systematic errors and how we might evaluate them using a combination of data and Monte Carlo simulation. For many of the potential systematic effects described below, we will have to wait until we accumulate more Run II data before we can begin to make a reliable estimate of the impact of these effects on our sensitivity.

The systematic uncertainties can be classified into three categories:

1. signal rate;
2. background normalization and the shape of the $m_{b\bar{b}}$ distribution for the backgrounds;
3. the b-$\bar{b}$ dijet mass resolution function.

8.1 Uncertainties in the Signal Rate

Uncertainties in the signal rate are due to (1) uncertainties in the theoretical predictions of the WH and ZH production cross sections and in the branching fraction of $H \to b\bar{b}$ and (2) experimental uncertainties in detector acceptance and detection efficiencies. The detection

systematics include errors in the estimates of our efficiencies for the trigger, lepton identification, missing transverse energy requirements, jet requirements, and b-jet identification. Some of the systematics associated with detection efficiency of the signal are correlated with the background rates, *e.g.,* a change in b-tag efficiency changes the signal and backgrounds coherently. This should be taken into account when evaluating these types of systematics.

8.2 Uncertainties in the Backgrounds

We expect that the normalization of the various backgrounds and the determination of the shapes of the $m_{b\bar{b}}$ distributions from these backgrounds will be determined from a combination of data and Monte Carlo, depending on the background process. Below we describe how we might determine these normalizations and shapes for the different physics backgrounds.

***$t\bar{t}$*:** top quark pair production produces background to the $\ell\nu b\bar{b}$ and $\nu\nu b\bar{b}$ signatures when a real neutrino is produced. There are two topologies:

- **the lepton plus jets topology:** $t \to W^+b$, with $W^+ \to \ell^+\bar{\nu}$, and $\bar{t} \to W^-\bar{b}$, with $W^- \to q\bar{q}'$, resulting in a $\ell\nu b\bar{b}q\bar{q}'$ final state, and
- **the dilepton topology:** $t \to W^+b$, with $W^+ \to \ell^+\bar{\nu}$, and $\bar{t} \to W^-\bar{b}$, with $W^- \to \ell^{-\prime}\nu$, resulting in a $\ell\ell'\nu\bar{\nu}b\bar{b}$ final state.

A dilepton event in which one (both) of the charged leptons is not identified produces background to the $\ell\nu b\bar{b}$ ($\nu\nu b\bar{b}$) signature. It should be possible to evaluate the rate of this background and the shape of the $m_{b\bar{b}}$ distribution for this background from identified top dilepton events. The statistics of these identified events will probably determine the most important systematic uncertainty on this background to the signal. The lepton plus jets topology is a background to the $\ell\nu b\bar{b}$ when one or both of the jets from the W decay do not satisfy the jet selection criteria and the event is not eliminated by the jet multiplicity requirement. In the case of the $\nu\nu b\bar{b}$ signature, the lepton plus jets topology is a background when the charged lepton is not identified. Again it should be possible to determine the normalization of this background and the shape of the $m_{b\bar{b}}$ distribution for this background from identified lepton plus jet events. In all of the cases described above, it will probably be necessary to use Monte Carlo simulations to determine the relative rate of identified top signal to unidentified top events that are background to the Higgs boson signal.

***W/Z* + jets:** The rate of W and Z production with associated jets from higher order QCD diagrams is much larger than the signal process, so we can treat the inclusive (no b tag) W/Z + jets data as a pure background sample. Almost all of the background to the Higgs boson signatures from this process is when the associated jets contain heavy flavor, either c or b jets. The rate of this background is determined from the rate of W/Z + jets in the data multiplied by the fraction of these events that contain heavy flavor jets. This fraction is determined from Monte Carlo, and there will be a systematic error associated with this fraction. The dijet mass spectrum observed in the W/Z + jets will be dominated by jets that are not due to heavy flavor. By comparing the single tagged, double tagged, and untagged dijet mass spectra, we can determine from the data whether the E_T spectrum of

the light quark and heavy flavor jets are different. Using a combination of data and Monte Carlo we can take into account the differences of b jets compared to light quark and gluon jets, and predict the expected dijet mass spectrum from heavy flavor. Again there will be a systematic uncertainty associated with this prediction.

Single top quark production: This is a particularly difficult background to evaluate, since the measurement of this background is based on a signature that is very similar to the Higgs boson signature. For example, $W^{*+} \to t\bar{b}$, followed by $t \to W^+b, W^+ \to \ell^+\bar{\nu}$ produces exactly the $\ell\nu b\bar{b}$ signature. We will have to rely on Monte Carlo simulation to predict the shape of this background in $m_{b\bar{b}}$ and allow the fit to the $m_{b\bar{b}}$ distribution to determine the normalization of this background. There will be systematic uncertainties associated with the predicted shape of the $m_{b\bar{b}}$ distribution from this background. The effect of floating this background in the fit of the $m_{b\bar{b}}$ distribution is not included in the results cited above.

***WZ, ZZ*:** This process forms background to the Higgs boson signature when $W \to \ell\nu$ and $Z \to b\bar{b}$ and $Z \to \nu\bar{\nu}$ and $Z \to b\bar{b}$. The purely leptonic topologies from these processes (*e.g.*, $W \to \ell\nu$ and $Z \to \ell\ell$) should be very low background and could be used to normalize the rate of these backgrounds. The numbers of these events, however, will be small, so if we use these events to measure the rates of WZ and ZZ production, there will be a significant statistical uncertainty in the measurement, which becomes a systematic uncertainty in the determination of the contribution of this background to the Higgs sample. It may be possible to reduce this statistical uncertainty by relating the production of WZ and ZZ to the higher rate of WW using theory. If the statistical uncertainty is too large, we may be forced to rely on a theoretical calculation of this background rate and there will be an associated systematic with this prediction. Whether or not we can normalize this background to the data, we will need to determine the distribution of $m_{b\bar{b}}$ from Z decay as well. The plan is to use data to measure this decay and determine this distribution.

QCD production of $b\bar{b}$ This is an important background to the $\nu\nu b\bar{b}$ Higgs boson signature. A method to estimate this background with the currently available Run IIA data samples and triggers is presented in detail in Section 3.8. There are several sources of systematic uncertainties in this study including the Monte Carlo estimate of the b content of the selected QCD sample, the b-tagging efficiencies and the luminosity normalization. As more Run IIA statistics is collected, the sidebands in $b\bar{b}$-dijet mass distribution of the selected sample will have competitive normalization errors to the rate measurement presented in Section 3.8. The sideband statistics of a loosely selected search sample with therefore be a limiting factor on the systematic error of the QCD acceptance. The current estimate of the number of QCD events in the ZH outside of the mass window is approximately 50 events per fb^{-1} following roughly the $100\%/\sqrt{B}$ estimate above 2 fb^{-1}.

8.3 Dijet Mass Resolution

Studies of the b-$\bar{b}$ dijet mass distribution described in Section 5 indicate that it may be possible to achieve a core resolution of 10%. This will be verified by studying resonant

decays $Z \to b\bar{b}$ in the data. In this study we have evaluated how the sensitivity changes if we are not able to achieve 10% mass resolution. We find that for a degradation of 20% in the mass resolution (*e.g.*, 10% becomes 12%), that the required integrated luminosity to achieve the same statistical statement increases by 20%. The dijet mass resolution may contain non-Gaussian tails or it may be described by more than one Gaussian. We have not evaluated how these possibilities affect our sensitivity. Eventually we will use the $Z \to b\bar{b}$ data to measure these non-Gaussian tails and there will be a systematic associated with the limitations of our determination of the resolution function from the data.

8.4 Cross Section Uncertainties

The search sensitivity estimates given in this report assume that the values of the background cross sections are perfectly known. There are varying degrees of accuracy in the cross section calculations depending on the type of process being computed. The previous sections discuss methods of determining the cross sections with complementary data samples. These measurements may result in cross section values that differ from those used in this study. As long as the cross sections are measured accurately, shifts in the values of the cross sections do not strongly affect the sensitivity results. Figure 25 shows the variation in the median value of the luminosity threshold for 3σ evidence for a Higgs boson of $m_H = 115$ GeV/c^2. The sensitivity versus luminosity depends roughly on S^2/B predicting a near-linear dependence on the number of background events, B. This relationship is well described in Figure 25 giving a 9% luminosity threshold shift for a 10% shift in the cross section. The signal dependence behaves quadratically.

There is an important distinction between searching for a new particle in a data sample with known background cross sections and searching in a sample in which there is uncertainty in the value of one or several of these cross sections. This uncertainty can arise from a limited data sample from which to determine the cross section in addition to weak theoretical guidance on how to predict the value. In general, if the background is in a sideband of the signal region, then the uncertainty on this background will go down with the statistical error as described in the beginning of this section. If the process cannot be distinguished from the signal, than this is an irreducible uncertainty. The effect of Gaussian irreducible uncertainties is estimated in Table 22 for signal and background cross sections. The dependence on the background uncertainty is stronger than a corresponding shift in the cross section value. A 10% uncertainty on the background increases the required luminosity for a 3σ excess by about 15%. The smaller effect from systematics relative to the SHWG study is ascribed to the use of the full mass spectrum in the sensitivity calculation described in Section 6.

9 Conclusions and Summary

The results of this study show a reduction in the amount of integrated luminosity required to search for the Higgs boson at the Tevatron collider relative to the previous SUSY-Higgs Working Group study. The following improvements were verified with detailed analyses:

- The efficiencies of triggers, lepton identification, as well as other selection criteria, are based on Run II data. The b-tagging efficiencies, one of the most crucial perfor-

Signal Uncertainty(%)	Background Uncertainty(%)	95% CL	3σ	5σ
0.00	0.00	1.75	4.17	10.98
0.00	0.05	1.84	4.38	12.04
0.00	0.10	1.91	4.64	12.90
0.00	0.15	1.99	4.73	13.52
0.00	0.20	1.98	4.95	14.12
0.05	0.00	1.71	4.15	10.89
0.05	0.05	1.79	4.39	12.12
0.05	0.10	1.89	4.65	13.05
0.05	0.15	1.93	4.85	13.66
0.05	0.20	1.98	5.00	14.04
0.10	0.00	1.66	4.27	11.09
0.10	0.05	1.82	4.56	12.38
0.10	0.10	1.82	4.79	13.18
0.10	0.15	1.93	4.92	13.82
0.10	0.20	2.02	5.13	14.26
0.20	0.00	1.58	4.69	11.34
0.20	0.05	1.63	4.92	12.77
0.20	0.10	1.82	5.15	13.53
0.20	0.15	1.94	5.35	14.13
0.20	0.20	2.09	5.50	14.76

Table 22: The change in luminosity thresholds in fb^{-1} for 95% exclusion, 3σ evidence and 5σ discovery for a Higgs boson with $m_H = 120$ GeV/c^2 for several values of Gaussian correlated uncertainties on signal and background cross sections. The thresholds are calculated using the Bayesian technique.

mance parameters in the search for the Higgs boson, are based on `GEANT` simulations of the Run IIA and Run IIB detectors and projected luminosities and have been tied to Run IIA data.

- The study of the dijet mass resolution in the $\ell\bar{\nu}b\bar{b}$ analysis indicates that a mass resolution of 10% may be experimentally achievable.
- The accuracy of the QCD background estimate in the $\nu\bar{\nu}b\bar{b}$ analysis was substantially improved by applying the event selection to the Run II data and using Monte Carlo generators to estimate the b-quark content.
- An advanced neural network analysis reduces dramatically the amount of $t\bar{t}$ background while keeping a large fraction of the signal.
- The use of the shapes of the signal and background distributions gives an enhancement in the search sensitivity of approximately 20% in equivalent integrated luminosity.

The WH and ZH search modes were combined to estimate the full sensitivity of a DØ and CDF data analysis with 1–10 fb^{-1} in the mass range 110–130 GeV/c^2. These results are summarized in Figure 24 and Table 21. A critical feature of these predictions is the ability to control systematic errors, especially on the dijet mass shape, for the signal and the backgrounds. Methods for controlling one of the primary classes of systematic uncertainty, namely, background rate uncertainties, are discussed. It is anticipated that further evaluation of the available data samples will give accurate estimates of several important background rates and detector efficiencies. In summary, the improvements in the Higgs search sensitivities come from a better use of signal information and more optimized methods of analysis. Further developments of this type are foreseen in a full complement of analyses from the two experiments.

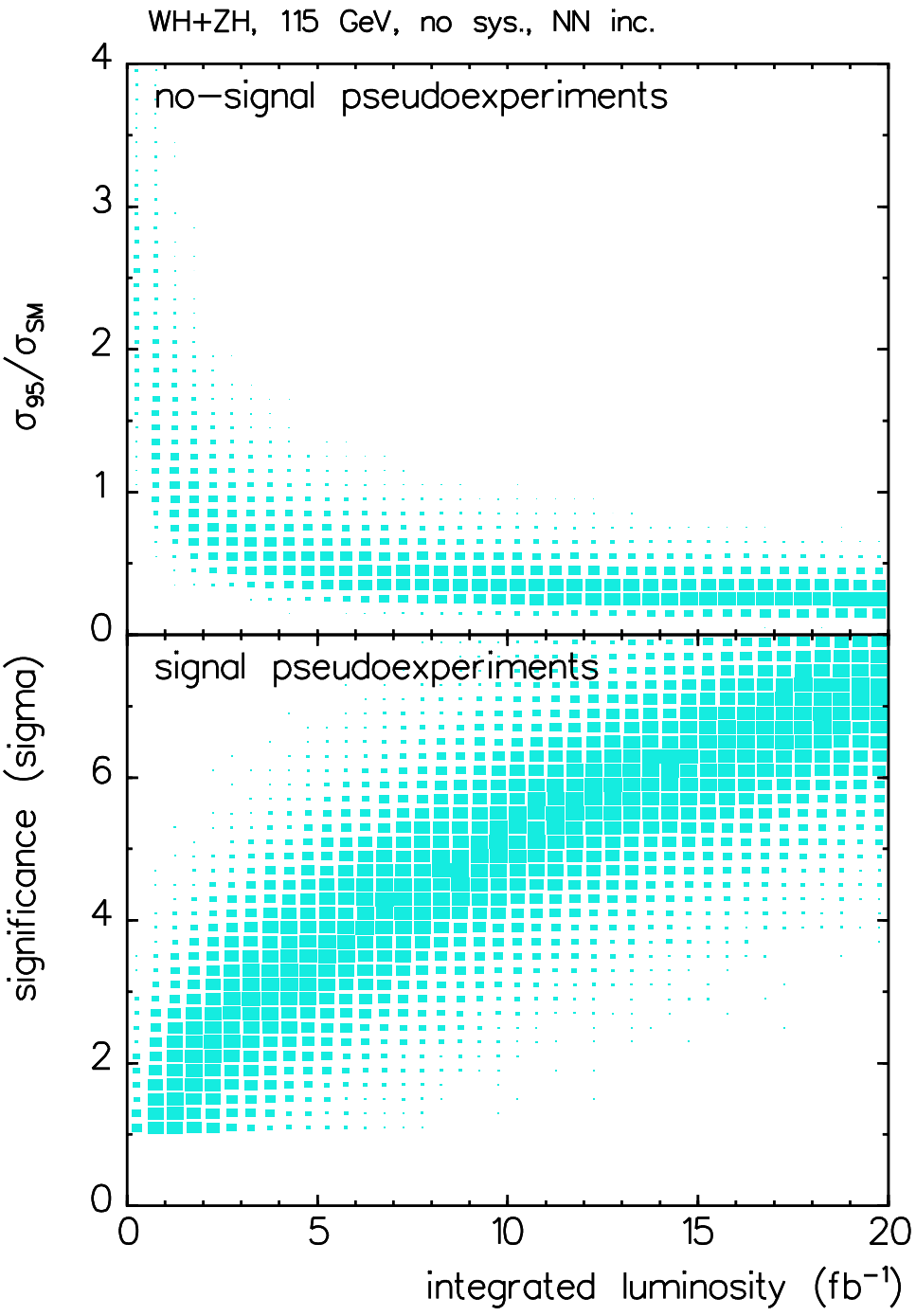

Figure 19: Top Plot: Scatter of pseudoexperiments using the Bayesian method. The plot shows the extracted 95% CL upper limit on the standard model cross section of a 115 GeV/c^2 Higgs boson as a function of integrated luminosity. The y-axis is normalized so 1.0 equals the standard model predicted cross section. The pseudoexperiments do not contain any signal. Bottom Plot: Scatter of pseudoexperiments using the Bayesian method. The plot shows the significance of the excess of events in the signal region versus integrated luminosity. Pseudoexperiments above 3.0 have more than a 3σ excess of events. These results are for the WH and ZH channels for both experiments combined. In both plots the integrated luminosity is *per* experiment.

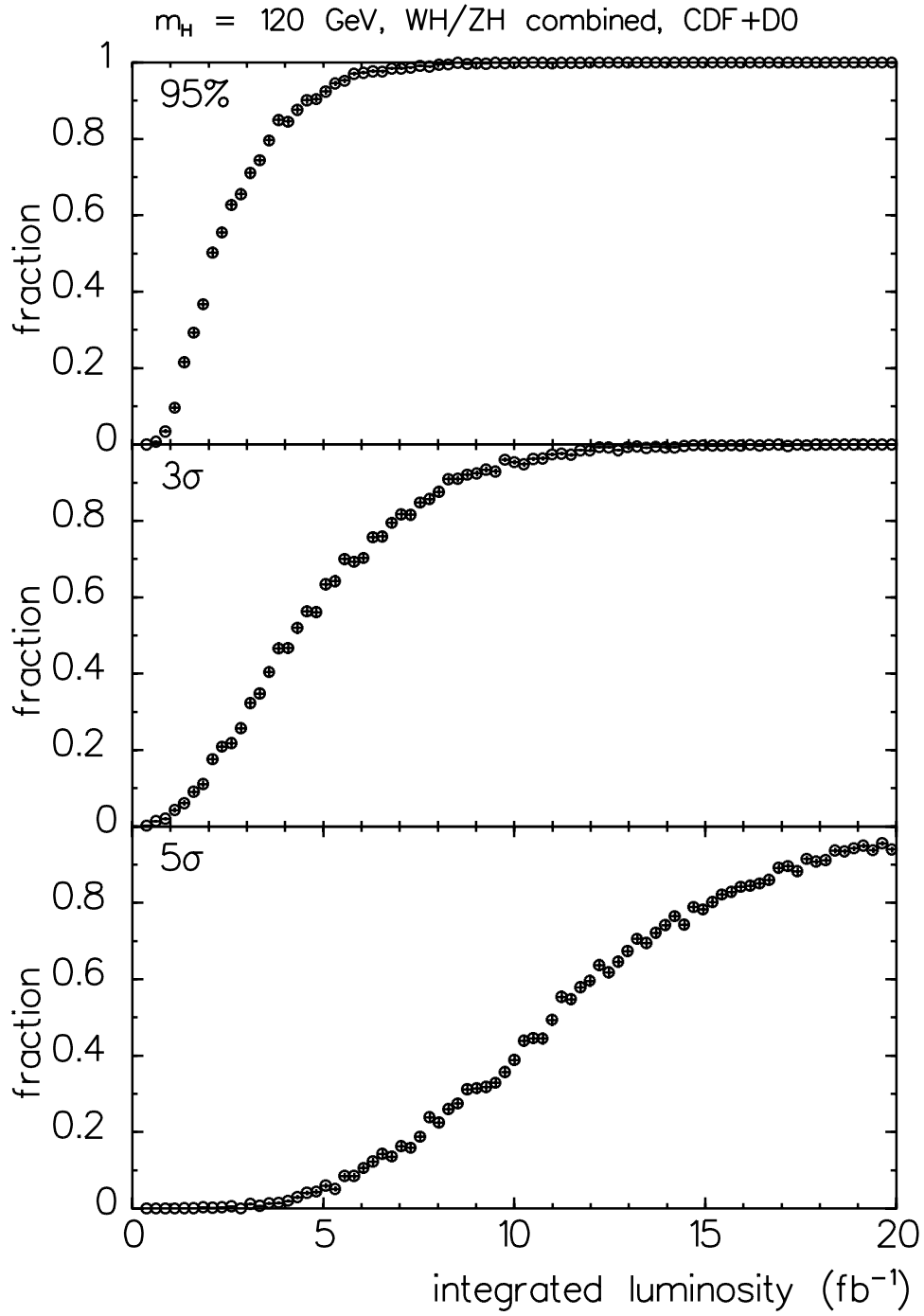

Figure 20: The fraction of pseudoexperiments from the Bayesian method that satisfy the three results criteria. This is for a Higgs mass of 120 GeV/c^2 and is the combination of the WH and ZH channels. The rates include scale factors for the inclusion of the $ZH \to \ell\ell\nu\nu$ channel and a factor for the optimization of the WH channel (see text). The integrated luminosity is *per* experiment.

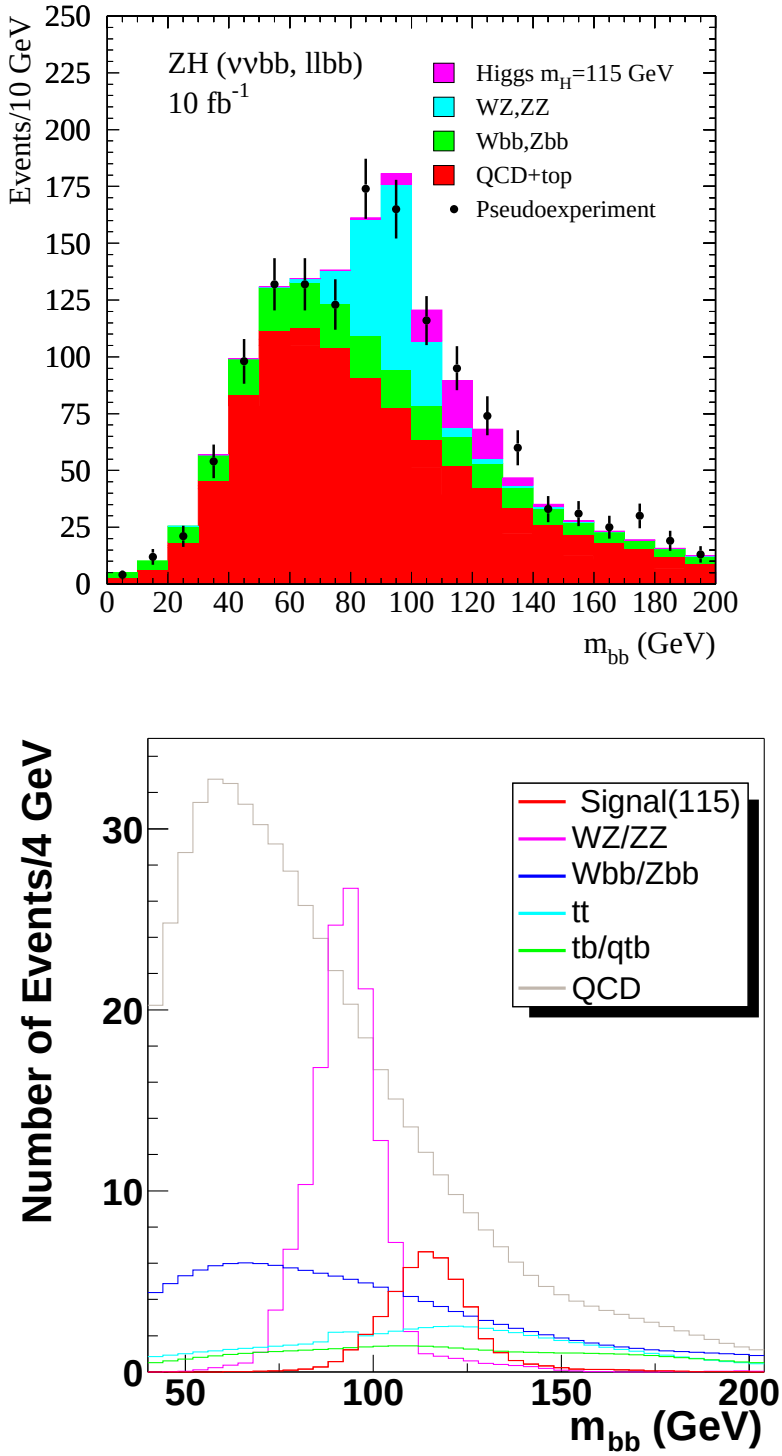

Figure 21: Mass distributions for the $\nu\bar{\nu}b\bar{b}$ analysis with $m_H = 115$ GeV/c^2. The top plot represents the expected mass distribution from a single experiment with 10 fb^{-1} of integrated luminosity. The bottom plot contains the signal and background shapes separately.

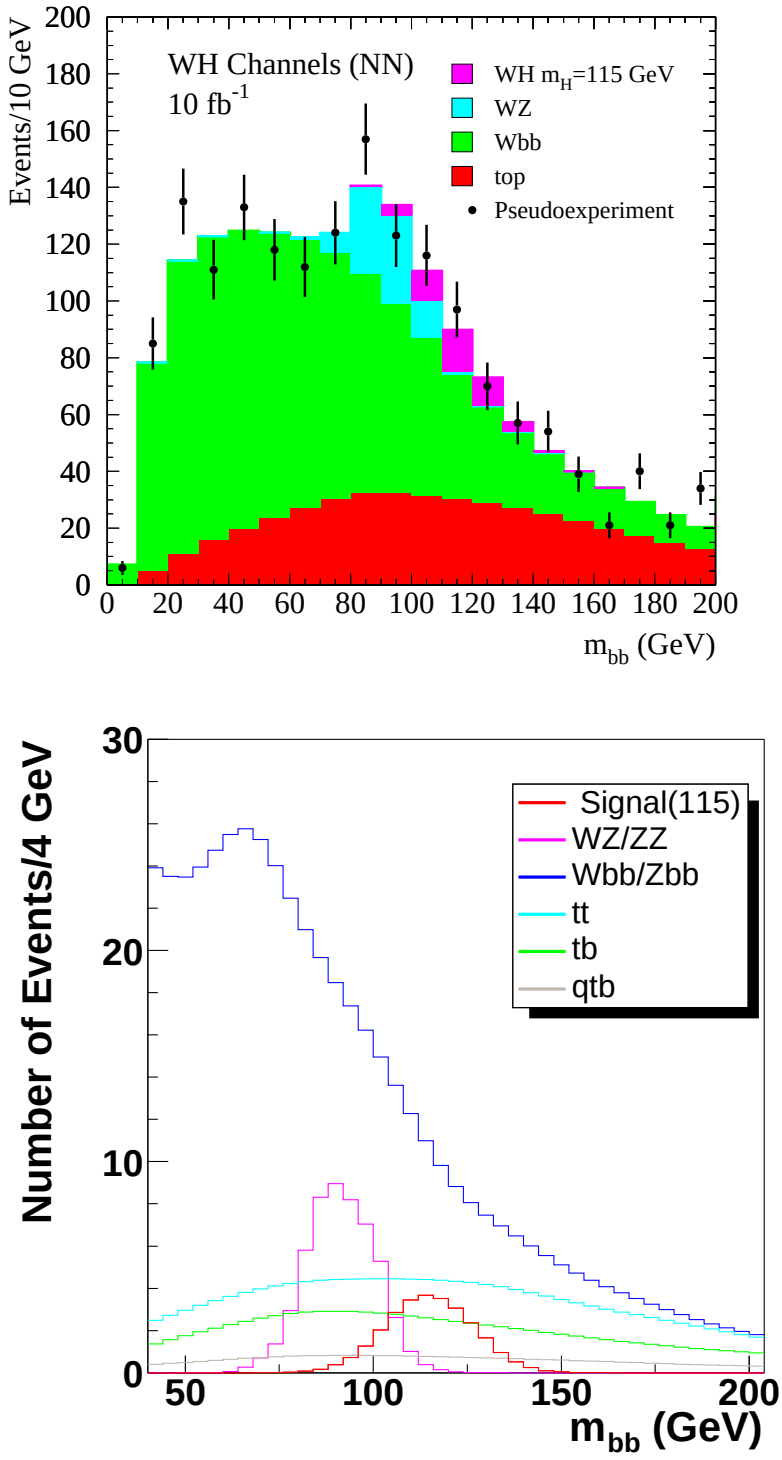

Figure 22: Mass distributions for the $\ell\bar{\nu}b\bar{b}$ analysis with $m_H = 115$ GeV/c^2 and neural network efficiencies applied. The top plot represents the expected mass distribution from a single experiment with 10 fb^{-1} of integrated luminosity. The bottom plot contains the signal and background shapes separately.

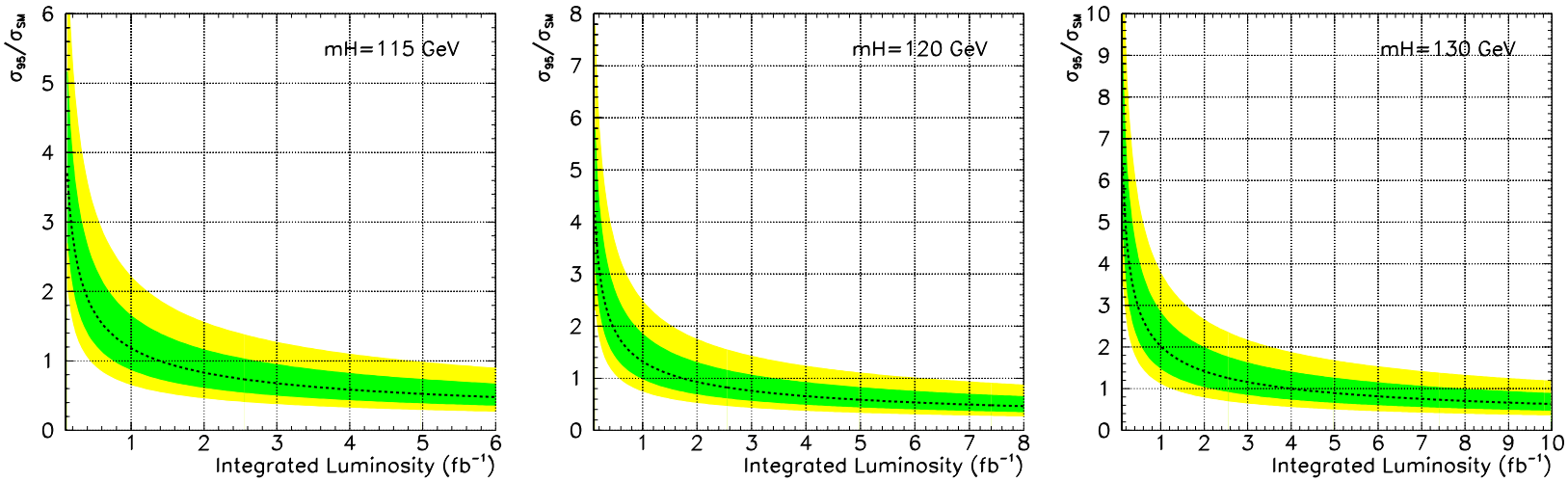

Figure 23: The 95% CL upper limit on the cross section for a Higgs of mass 115,120, and 130 GeV/c^2. The technique combines both the WH and ZH channels and uses the CL_s method for the extraction of the limit. The y-axis is normalized so that 1.0 corresponds to the standard model cross section. The dashed line show the median for the pseudoexperiments. The green (inner) envelope encloses 68% of the pseudoexperiments and the yellow (outer) envelope encloses 95% of the experiments. The rates include scale factors for the inclusion of the $ZH \to \ell\ell\nu\nu$ channel and a factor for the optimization of the WH channel (see text).

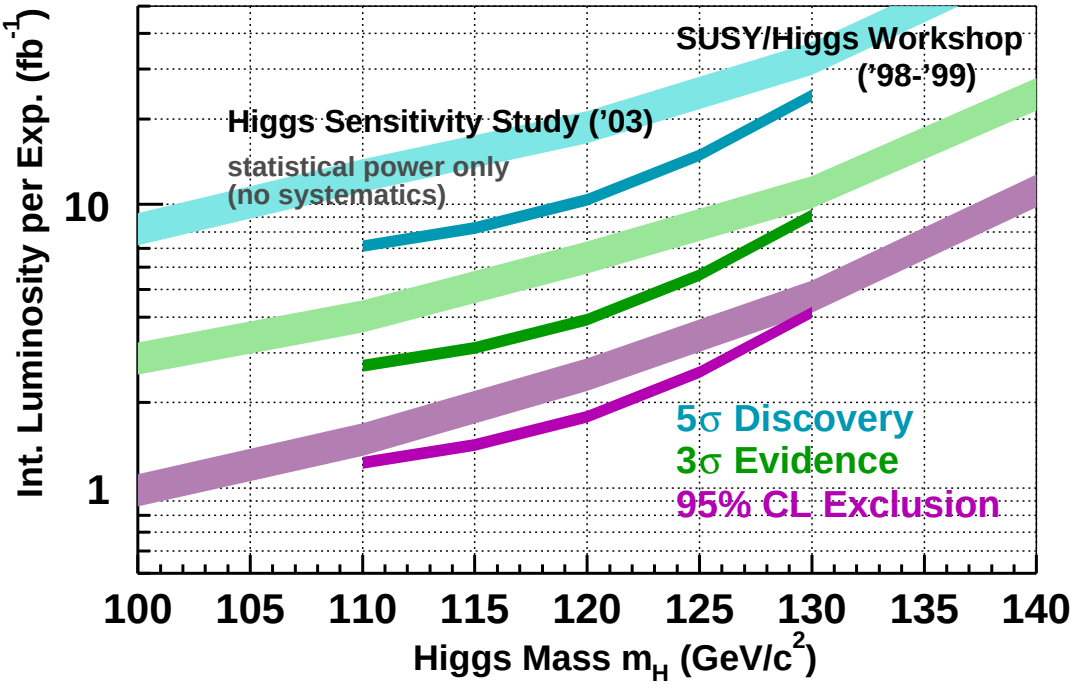

Figure 24: Integrated luminosities per experiment corresponding to the median expectations for 95% confidence level exclusion, 3σ evidence and 5σ discovery for $m_H = 110-130$ GeV/c^2. The narrow curves are the updated analysis from this study (2003) and the thicker curves are the results from the previous SHWG Study (1999).

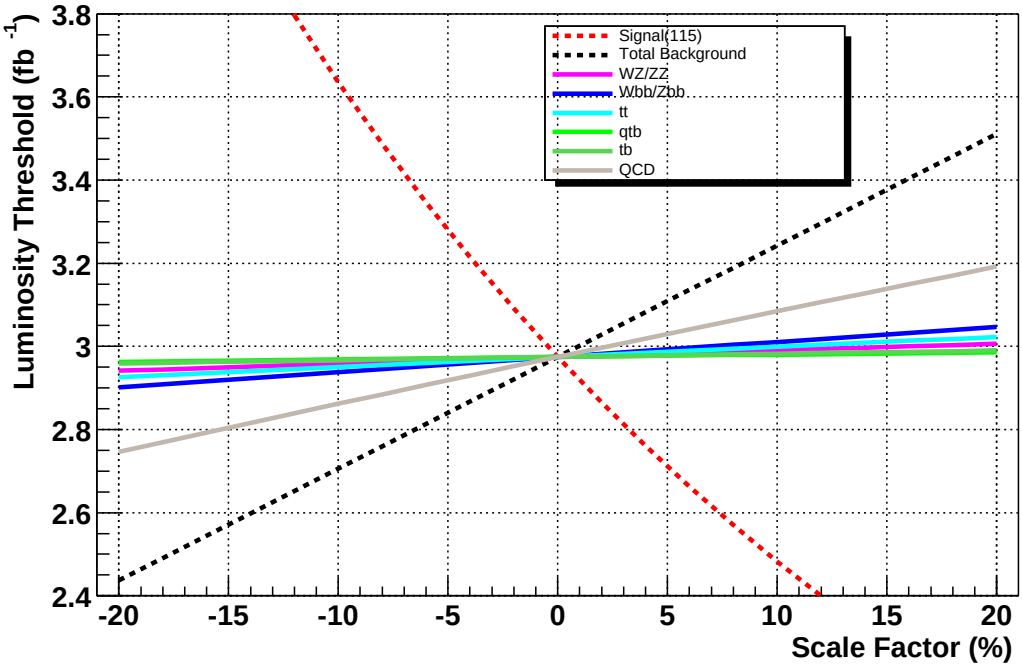

Figure 25: The variation in the median value of the luminosity threshold for 3σ evidence for a Higgs boson of $m_H = 115$ GeV/c^2 is plotted for percentage shifts in the background and signal cross section values.

References

[1] P.W. Higgs, Phys. Rev. Lett., **12**, 132 (1964).

[2] M. Carena, J. S. Conway, H. E. Haber, J. D. Hobbs, *et al*, "*Report of the Higgs Working Group of the Tevatron Run 2 SUSY/Higgs Workshop"*, hep-ph/0010338.

[3] T. Han, S. Willenbrock, Phys. Lett. **B273**, 167 (1991).

[4] A. Djouadi, K. Kalinowski, M. Spira, Comp. Phys. Commun. **108C**, 56 (1998).

[5] The CDF Collaboration, T. Affolder *et al.*, Phys. Rev. **D64**, 032002 (2001).

[6] A.S. Turcot, "*A Trigger Strategy for Associated Higgs Boson Production at* $\mathcal{L} = 2 \times 10^{32}$ cm^{-2} s^{-1}*"*, DØ Note 4186.

[7] The DØ Collaboration, V.M. Abazov *et al.*, "Run IIB Upgrade Technical Design Report", Sept 12, 2002, Section 7.4, and Figure 83, page. 438.

[8] B. Knuteson *et al.*, "*P(met): The Missing Transverse Energy Resolution of an Event"*, DØ Note 3629.

[9] The DØ Collaboration, R.D. Field *et al.*, Phys. Rev. **D55**, 5685 (1997).

[10] University of Stuttgart, http://www-ra.informatik.uni-tuebingen.de/SNNS.

[11] A. Khanov, M. Narain, F. Rizatdinova, "*Study of reconstruction efficiency, b-tagging efficiency and mis-tag rates in Run2b"*, DØ Note 4239.

[12] The DØ Collaboration, V.M. Abazov *et al.*, Phys. Rev. Lett., **88**, 191801 (2002).

[13] A. Goussiou, "*Dijet Mass Resolution"*, DØ Note 4189.

[14] T. Dorigo, *"Observation of Z Decays to b Quark Pairs at the Tevatron Collider"*, hep-ex/9806022.

[15] A. L. Read, *"Modified Frequentist Analysis of Search Results (The* CL_s *Method)"*, in the proceedings of the 1st Workshop on Confidence Limits, January 2000, Geneva, Switzerland, CERN Yellow Report CERN 2000-005.